CEA
C.E. SACLAY
DSM

SERVICE D'ÉTUDE DES ACCÉLÉRATEURS

Sx 9437

CEA/DAPNIA/SEA 94 11   07/1994
à   CEA/DAPNIA/SEA 94 15
et CEA/DAPNIA/SEA 94 17
à   CEA/DAPNIA/SEA 94 22

Communications à EPAC 94

DAPNIA

Couverture Sylvie Cabrit et Marc Sauvage

Le DAPNIA (**D**épartement d'**A**strophysique, de physique des **P**articules, de physique **N**ucléaire et de l'**I**nstrumentation **A**ssociée) regroupe les activités du Service d'Astrophysique (SAp), du Département de Physique des Particules Elémentaires (DPhPE) et du Département de Physique Nucléaire (DPhN).

Adresse :   DAPNIA, Bâtiment 141
                   CEA Saclay
                   F - 91191 Gif-sur-Yvette Cedex

Contributions à :

4th European Particle Accelerator Conference

Queen Elizabeth II Convention centre, London,

Grande Bretagne

27 juin au 1 Juillet 1994

QUADRUPOLAR WAKEFIELD INDUCED SINGLE-BUNCH EMITTANCE GROWTH IN LINEAR COLLIDERS

S. Fartoukh, O. Napoly

Quadrupolar Wakefield Induced Single-Bunch Emittance Growth in Linear Colliders

Stéphane FARTOUKH, Olivier NAPOLY

CEA, DSM/DAPNIA/Service d'Etudes des Accélérateurs

CE-Saclay, F-91191 Gif-sur-Yvette CEDEX, France

Abstract

Emittance dilution can be induced in linear colliders by the short range quadrupolar wakefields generated, even in perfectly aligned accelerating structures, by the charge distribution of flat beams. We consider a linac with a constant phase-advance FODO lattice and we calculate, for different energy scaling laws of the beta functions along the linac, the single-bunch transverse emittance growths for a two-particle model where the bunch is represented by a head and a tail centered beam ellipse. We analyze the implication of this effect for the linar collider designs.

1 INTRODUCTION

Preserving the beam transverse emittances from being degraded along the linacs in order to reach the design luminosity at the interaction point is a major challenge of the future linear collider design. Many years ago, quadrupole wakefields were recognized as a possible source of emittance dilution [1] along the linac of the SLAC linear collider. Quadrupole wakefields are induced by the beating of the horizontal and vertical beta-functions which, even for round beams, generates a non-zero transverse charge quadrupole moment proportional to the beam averaged $\langle x^2 \rangle - \langle y^2 \rangle$. They in turn create a quadrupole gradient focusing error along the beam, which modifies the designed beam transport optics of the linac. However, it was soon realized that dipole wakefields are the dominant source of emittance growth. This is essentially due to the facts that, first the dipole transverse wake potential grows more rapidly with respect to the transverse coordinates (that is linearly rather than quadratically for the quadrupole one) and, second the quadrupole moment of round beams rapidly averages to zero along the linac.

In the next linear collider the obligation, related to beamstrahlung, to accelerate flat beams with a large horizontal to vertical emittance ratio reinforces the expected effect of quadrupole wakefields because the quadrupole moment, dominated by the horizontal average $\langle x^2 \rangle$, remains positive along the linac. Moreover, unlike the dipole one, the quadrupole wake of a centered beam accelerated along a perfectly aligned linac does not vanish. Since the single-bunch emittance growth is a collective effect proportional to N^2, where N is the bunch population, depending in an essential way on the injection energy and on the focalisation along the linac, it is important to know what is the maximum bunch charge which can be accelerated without degrading the transverse emittance for given injection energy and focalisation optics. This is the question we want to answer in this paper by calculating the single-bunch emittance growth induced by quadrupole wakefields in the framework of the "2 particle model" where the bunch is modeled by 2 beam ellipses representing the head and the tail of the bunch. We will consider a bunch injected on-axis in a perfectly aligned linac. We will assume FODO lattice with a *constant* phase-advance and a scaling of the FODO-lengths and beta-functions as E^α, where E is the energy along the linac.

2 CALCULATION OF THE EMITTANCE GROWTH

2.1 The 2-particle model

We consider a bunch formed by 2 slices separated by Δz. The two slices have identical beam matrix Σ_0 at injection. While the first slice obeys the design focalisation along the linac, the second one is affected by the quadrupole gradient induced by the quadrupole wake of the first slice in the accelerating structures. Their beam matrices Σ_1 and Σ_2 therefore differ at the linac exit, although their emittances stay equal. Parametrizing a beam matrix as

$$\Sigma = \epsilon \left(\begin{array}{cc} \beta & -\alpha \\ -\alpha & \gamma \end{array} \right)$$

with $\epsilon = \sqrt{\det \Sigma}$ the emittance, the total emittance of the bunch is given by

$$\epsilon_b = \sqrt{\det \left(\frac{\Sigma_1 + \Sigma_2}{2} \right)} = \epsilon_1 \sqrt{1 + \frac{1}{4}(\delta\alpha^2 - \delta\beta \, \delta\gamma)}$$

where $\delta\alpha$, $\delta\beta$ and $\delta\gamma$ are the differences of the α, β and γ parameters between the two slices. At the lowest order, the emittance growth is then given by

$$\frac{\delta\epsilon}{\epsilon} = \frac{1}{8}(\delta\alpha^2 - \delta\beta\delta\gamma)$$

2.2 Transverse motion with focusing error

The transverse motion of the first slice in the linac is governed by the Hill equation with an acceleration term

$$x'' + E'/E \, x' + K \, x = 0$$

where x represents either transverse coordinate, E' is the energy gradient and K the focusing gradient along the linac. We assume that the tail slice feels a focusing gradient δK due to the quadrupole wake from the head slice

in the accelerating structures [1]. Denoting by $R(s, s')$ the transfer matrix from position s' to s along the linac associated with the gradient K, and by $(R + \delta R)(s, s')$ the one associated with $K + \delta K$, one has

$$\delta\Sigma = \Sigma_2 - \Sigma_1 = \delta Q \cdot \Sigma_1 + \Sigma_1 \cdot \delta Q^\mathsf{T}$$

to first order in δR, with δQ the following matrix

$$\delta Q = \delta R(s_1, s_0) \cdot R^{-1}(s_1, s_0) \, ,$$

δQ^T its transpose, and s_0 and s_1 the beginning and end positions in the linac. The transfer matrix obeys the following differential equation

$$\partial_s R(s, s') = A(s) \cdot R(s, s')$$

with the matrix $A(s)$, deduced from Hill's equation, given by

$$A(s) = \begin{pmatrix} 0 & 1 \\ -K(s) & -(E'/E)(s) \end{pmatrix} \, .$$

The matrix δQ can be calculated by integrating the equation for the difference δR. Neglecting the difference $\delta(E'/E)$ in the accelerating gradient between the slices which originates from the RF-phase and the longitudinal wakefield, one gets at first order in δK

$$\delta Q = \int_{s_0}^{s_1} ds\, R(s_1, s) \cdot \delta A(s) \cdot R(s_1, s)^{-1} \, ,$$

with

$$\delta A(s) = \begin{pmatrix} 0 & 0 \\ -\delta K(s) & 0 \end{pmatrix} \, .$$

The above expression of δQ only involves the R_{12} and R_{22} matrix elements of $R(s_1, s)$, which can be written as

$$R_{12}(s_1, s) = \sqrt{\frac{E}{E_1}} \sqrt{\beta\beta_1} \sin(\Delta\psi)$$
$$R_{22}(s_1, s) = \sqrt{\frac{E}{E_1}} \sqrt{\frac{\beta}{\beta_1}} (\cos(\Delta\psi) - \alpha_1 \sin(\Delta\psi))$$

where $\Delta\psi$ is the phase advance from s to s_1. This leads to the following expression of the difference between the head and tail beam matrices

$$\delta\Sigma = \epsilon_1 \int_{s_0}^{s_1} ds\, \delta K(s)\, \beta(s) \begin{pmatrix} -\beta_1 \sin & \alpha_1 \sin - \cos \\ \alpha_1 \sin - \cos & \frac{\sin}{\beta_1}(1 + 2\alpha_1 \tan - \alpha_1^2) \end{pmatrix}$$

where the argument of the trigonometric functions is $2\Delta\psi$. The emittance growth at the lowest order in the gradient error δK is then simply given by

$$\frac{\delta\epsilon}{\epsilon} = \frac{1}{8} \left| \int_{s_0}^{s_1} ds\, \delta K(s)\, \beta(s) \exp(2i\Delta\psi) \right|^2 \, .$$

2.3 The quadrupole wake induced focusing error

As first discussed in [1], the quadrupole wakefields created by the first slice and averaged over a long accelerating section induce a transverse Laplace force given by

$$e(\vec{E} + \vec{v} \times \vec{B}) = N\, e^2\, w_2(\Delta z)\, Q_1 (x\hat{x} - y\hat{y})$$

with N the bunch population, $Q_1 = \langle x^2 \rangle - \langle y^2 \rangle$ the transverse quadrupole moment of the head slice, $\hat{x}$ and $\hat{y}$ the unit vectors in the x and y directions, and w_2 the average quadrupolar wake potential [2] of the accelerating structure, assumed axisymmetric, per unit length and unit charge. As in [1], we assume that there is no source of xy-coupling in the linac and we neglect the effect of the skew-quadrupolar wakefields proportional to $\langle xy \rangle$. For flat beams, the large horizontal over vertical emittance ratio allows the following approximation

$$Q_1(s) = \epsilon_x(s)\, \beta_x(s) - \epsilon_y(s)\, \beta_y(s) \simeq \epsilon_x(s)\, \beta_x(s)$$

Translated in the equation of motion, the above Laplace force gives rise to the following focusing gradient

$$\delta K(s) = -\frac{N\, e^2}{E(s)}\, w_2(\Delta z)\, \epsilon_x(s)\, \beta_x(s)$$

which we parametrize as $\delta K(s) = -A(s)\beta_x(s)$ for later convenience. Notice that the coefficient $A(s)$ scales like the inverse of the energy squared along the linac.

2.4 Emittance Growth after one FODO cell

The emittance growth after one FODO cell can be easily calculated by assuming that the energy is constant over the cell and that the beam is matched. In fact, we consider a cell with μ phase-advance starting by either half a focusing quadrupole F/2 or half a defocusing one D/2. The horizontal and vertical emittance growths are then given by

$$\frac{\delta\epsilon_{x,y}}{\epsilon_{x,y}} = c_{x,y}^2 \frac{A^2 L^6}{2}$$

where L is the distance between two quadrupoles. The coefficients c_x and c_y depend on the phase advance and on the cell type. As shown in Table 1 for 60° and 90° phase advances, they are always of the order of one.

Table 1: Coefficients $c_{x,y}$ for the single cell emittance growth.

μ	c_x at F/2	c_y at F/2	c_x at D/2	c_y at D/2
60°	3.37	-1.73	4.63	-1.25
90°	0.727	-1.66	3.27	-1.00

2.5 Emittance Growth over the linac

To calculate the emittance growth over the linac, we assume that the phase advance per cell μ is constant along the linac while the length L scales as $L_0(E/E_0)^\alpha$, E_0 being the injection energy and L_0 the distance between two quadrupoles in the first cell. To simplify the calculation, we also assume that the linear rise of the energy along the linac is slow compared to the beta-wavelength

$$E'/E \ll 1/2L \, .$$

The energy can then be approximated by a step function such that it is constant and the beam is assumed to

Table 2: 500 GeV c.m. energy linear collider parameters and characteristic length L_c for $E_0 = 5$ GeV.

	CLIC	VLEPP	NLC	SBLC	TESLA
f_{RF} [GHz]	30	14	11.4	3	1.3
N [10^9]	6	200	6.5	29	50
$\gamma\epsilon_x$ [10^{-6}m]	1.8	20	5	10	20
σ_z [μm]	170	750	100	500	1000
$W(2\sigma_z)$ [cm^{-5}]	4×10^4	560	200	0.3	
$w_2(2\sigma_z)$ [V/C m]	3.6×10^{24}	5.0×10^{22}	1.8×10^{22}	2.7×10^{19}	5.0×10^{16}
L_c [m]	20	12	81	340	1830

be matched in every cell. Since the beta functions scale like the length L, the gradient error δK then scales as $\delta K_0 (E/E_0)^{\alpha-2}$ where δK_0 is the gradient error in the first cell. The integral over the linac entering in the expression of the emittance growth can then be replaced by a sum over the N FODO cells composing the linac, leading to

$$\frac{\delta\epsilon}{\epsilon} = \frac{1}{8} \left| \sum_{n=1}^{N} e^{2in\mu} \left(\frac{E_n}{E_0}\right)^{3\alpha-2} \int_{s_0}^{s_0+2L_0} ds\, \delta K_0(s)\, \beta_0(s)\, e^{2i\Delta\psi} \right|^2 .$$

The emittance growth over the linac is therefore equal to the emittance growth after the first cell $(\delta\epsilon/\epsilon)_0$ times a correction factor as given by

$$\frac{\delta\epsilon}{\epsilon} = \left(\frac{\delta\epsilon}{\epsilon}\right)_0 \left| \sum_{n=1}^{N} e^{2in\mu} \left(\frac{E_n}{E_0}\right)^{3\alpha-2} \right|^2 .$$

For an infinite number of cells, the above alternating sum diverges when $\alpha > 2/3$, oscillates when $\alpha = 2/3$, and converges when $\alpha < 2/3$. This clearly shows the special role of the $\alpha = 2/3$ scaling, independently of the value of the phase advance μ. For finite N, the sum can be easily evaluated when μ is a submultiple of 2π. In particular, for 90° phase advance, writing

$$\left(\frac{E_{n+1}}{E_0}\right)^{3\alpha-2} - \left(\frac{E_n}{E_0}\right)^{3\alpha-2} \simeq (3\alpha-2)\frac{2L_n E'}{E_0}\left(\frac{E_n}{E_0}\right)^{3\alpha-3}$$

and then replacing the sum over the cells back to an integral over the linac, leads to

$$\frac{\delta\epsilon_{x,y}}{\epsilon_{x,y}} = c_{x,y}^2 \frac{A_0^2 L_0^6}{8} \left\{ \begin{array}{ll} \left(\left(\frac{E_1}{E_0}\right)^{3\alpha-2} - 1\right)^2 & \text{if } \alpha \neq \frac{2}{3} \\ (1-(-1)^N)^2 & \text{if } \alpha = \frac{2}{3} \end{array} \right.$$

where E_1 is the beam energy at the end of the linac. When $E_1 \gg E_0$, the emittance growth scales like $(E_1/E_0)^{6\alpha-4}$ if $\alpha > 2/3$, and is independent of E_1 if $\alpha \leq 2/3$. From the above discussion on the $N \to \infty$ convergence, the critical exponent $2/3$ does not depend on the value of the phase advance. In fact the emittance growth for 60° phase advance is given by the 90° result divided by $\sin^2(\pi/3)$.

3 IMPLICATION FOR LINEAR COLLIDER DESIGNS

To evaluate the magnitude of this effect for the linear collider designs, we introduce the characteristic length L_c as

$$L_c = A_0^{-1/3} = \left(\frac{N e^2 w_2(\Delta z)\, \epsilon_x(s_0)}{E_0}\right)^{-1/3} .$$

The emittance growth induced by quadrupole wakefields then reads

$$\frac{\delta\epsilon_{x,y}}{\epsilon_{x,y}} = \frac{c_{x,y}^2}{8}\left(\frac{L_0}{L_c}\right)^6 \left\{ \begin{array}{ll} \left(\left(\frac{E_1}{E_0}\right)^{3\alpha-2} - 1\right)^2 & \text{if } \alpha \neq \frac{2}{3} \\ (1-(-1)^N)^2 & \text{if } \alpha = \frac{2}{3} \end{array} \right. .$$

so that it is small only when $L_0 \ll L_c$. The length L_c is given in Table 2 for all linear colliders (except JLC for which the RF frequency is not yet known) assuming an injection energy $E_0 = 5$ GeV. The wake potential w_2, evaluated for $\Delta z = 2\sigma_z$, has been calculated with TBCI [2] for TESLA and, for the other designs, derived from the wake function $W = 4\pi\epsilon_0 w_2$ given in [1] for the SLC 3 GHz cavities down to a distance of 3 mm. For RF frequencies f_{RF} higher than 3 GHz, we used the following scaling formula

$$W^{(f_{RF})}(2\sigma_z) = \lambda^5\, W^{(3\,\text{GHz})}(2\lambda\sigma_z)$$

with $\lambda = f_{RF}/3\,\text{GHz}$.

As shown by Table 2, the emittance growth can be sizeable for the designs with the highest RF frequency. This is even more true if the linac optics scales linearly with energy ($\alpha = 1$) due to the correction factor $(E_1/E_0)^2$.

4 CONCLUSION

Using a simple "2 slice model", we have estimated at the lowest order in the wake potential the emittance growth induced by the transverse quadrupole wakefields for a flat bunch accelerated in a perfectly aligned linac. The emittance growth increases quadratically with the population and the horizontal emittance of the bunch. It depends also strongly on the injection energy E_0 and the linac focalisation optics. Assuming that the half beta-wavelength is given by $L_0(E/E_0)^\alpha$ as a function of the energy E along the linac, the emittance growth is proportional to $(L_0/L_c)^6$ with a correction factor $(E_1/E_0)^{6\alpha-4}$ when $\alpha > 2/3$. The characteristic length L_c sets a lower limit on the beta-wavelength close to 20 meters, and even below for $\alpha = 1$, for the highest RF-frequency linear collider designs.

5 REFERENCES

[1] A.W. Chao and R.K. Cooper, "Transverse Quadrupole Wake Field Effects in High Intensity Linacs", Particle Accelerators, vol. 13, pp. 1–12, 1983

[2] T. Weiland, "Comment on Wake Field Computation in Time Domain", NIM, vol. 216, pp. 31–34, 1983

FFADA COMPUTER DESIGN OF FINAL FOCUS
SYSTEMS FOR LINEAR COLLIDERS

O. Napoly, B. Dunham

FFADA
Computer Design of Final Focus Systems for Linear Colliders

Olivier NAPOLY, Bruce DUNHAM

CEA, DSM/DAPNIA/Service d'Etudes des Accélérateurs

CE-Saclay, F-91191 Gif-sur-Yvette CEDEX, France

Abstract

FFADA, for Final Focus Automatic Design and Analysis, is a program which allows the user to automatically design a generic final focus system corresponding to a set of a few basic beam and machine parameters for linear colliders. It also derives the main properties of the designed system in terms of momentum acceptance, tracking, collimation requirements and Oide effect. Finally, the program analyzes the effect of magnet misalignment and field errors on the beam parameters and luminosity at the interaction point.

1 INTRODUCTION

Final focus systems (FFS) must reduce the colliding beam to nanometer spot sizes at the interaction point (IP) of future linear colliders. With the transverse emittances foreseen, the corresponding β^* are in the range of 0.1-1mm. The main difficulty is then to correct the chromatic aberrations which dominate the linear optics as soon as the energy spread is larger than β^*/l^*, where l^* is the distance separating the IP from the last focusing quadrupole. A generic system, adapted from the SLC final focus optics [1] has been derived [2, 3] which is free from 2nd and 3rd order aberrations. This solution is highly symmetric, provides several image points of the IP to monitor the beam, and contains the minimal number of four sextupoles (two non-interleaved pairs) for the chromatic correction. It is well adapted to designs where the beam energy spread is below 1% and, with additional sextupoles [4, 5], it can provide a larger energy acceptance.

The generic system is a telescopic transfer line which includes: a matching telescopic transformer (MT) with π-phase advance, achieving the first demagnification of the beam with two quadrupole doublets; a chromatic correction section (CCS); that is, a +1-transformer with 4π-phase advance including two sextupole pairs to cancel the second order chromatic aberrations generated mainly by the last focusing doublet; a final telescopic transformer (FT) achieving the final demagnification of the beam to the desired spot size at the IP, with π-phase advance again and two quadrupole doublets.

In this paper we describe the computer program FFADA which automatizes the operations needed to design and analyze such a generic final focus system. In this way, a FFS can be rapidly optimized for a set of basic beam and machine parameters, and adapted to later changes of these parameters. After generating the telescopic transfer line matched to second order, FFADA analyzes the following

properties:

1) the energy acceptance of the system, both analytically and by tracking;
2) the beta-functions and beam envelopes in the last doublet down to the IP;
3) the effect of the synchrotron radiation in the last doublet on the beam spot size [6] and the beam collimation requirements;
4) the sensitivity of the luminosity to beam transverse offset and dispersion at the IP;
5) the tolerances to misalignment and field errors of the magnets of the system.

FFADA runs under UNIX SystemV with FORTRAN and the optics code MAD [7] available. Its structure is modular so that new functions can be easily included. The results are presented in a few output files associated with each modules, and in a series of output files for graphics presentation. An extended presentation of the program FFADA can be found in [8].

2 INPUT PARAMETERS

For the sake of the presentation, we consider an hypothetical design for a "future linear collider", abbreviated to flc. The final focus sytem derived by FFADA and its properties are essentially determined by two input data files. The final focus optics depends on the optics and hardware parameters defined in the file flc.ffs, while the properties of the system, such as the bandwidth, the beam envelopes or the tolerances, are determined by the beam parameters given in the flc.beam.

```
                    FLC BEAM
Energy                          [GeV]    : 250.

Horizontal RMS at the IP        [nm]     : 100.
Vertical   RMS at the IP        [nm]     :  10.

Horizontal normalized emittance [m]      : 1.0e-6
Vertical   normalized emittance [m]      : 1.0e-8

Longitudinal RMS                [mm]     : 0.1
Relative energy RMS                      : 1.e-3
Energy profile case  [-1=linear, 0=zero] : 1

Bunch population                         : 1.0e+10
Repetition rate                 [Hz]     : 1.0e+2
```

Table 1 : Beam parameter definitions at the IP

2.1 Beam parameters

The desired beam parameters at the IP are defined in
flc.beam (see Table 1). The transverse and longitudi-
nal distributions are assumed Gaussian. The energy dis-
tribution is the superposition of an incoherent Gaussian
distribution and a coherent energy profile $\delta(z)$ along the
bunch which describes the combined effect of the RF accel-
erating phase and longitudinal wakefield. If not zero, the
energy profile $\delta(z)$ can be selected among several options
including linear or user defined profiles.

Input parameters for FFS

Total length of the FFS	[m] :	600.
Total horizontal demagnification	:	50.
Total vertical demagnification	:	100.

Parameters of Final Telescope

Horizontal FT demagnification	XM = -R22 :	10.
Vertical FT demagnification	YM = -R44 :	20.
Length of last drift	[m] :	3.0
Length of last but one drift	[m] :	0.35
Polarity of last quadrupole	:	D
Length of last quadrupole	[m] :	1.1
Pole-tip field of last doublet quads	[T] :	6.
Aperture diameter of last doublet quads	[mm] :	48.
Length of first drift	[m] :	1.
Length of first doublet quads	[m] :	0.3

Parameters of Matching Telescope

Polarity of last quadrupole	:	D
Maximum pole-tip field	[T] :	1.4
Aperture diameter of last quad	[mm] :	4.
Length of first drift	[m] :	0.5

Parameters of Microvertex Detector

Aperture diameter	[mm] :	30.

Table 2 : Optics and hardware parameters of the FFS

2.2 Optics and hardware parameters

The optics, layout and hardware parameters of the final
focus sytem which can be freely set are defined in flc.ffs
(see Table 2). However, some parameters will differ in the
final focus system derived by FFADA, namely: the total
length of the FFS and the length of the first drift of the 2
telescopes which are the values for the thin lens solution
first derived by FFADA, and are modified in the process of
matching it to a thick lens one; and, the length of the last
quadrupole of the final telescope which is used as a starting
value for the optimization of the final telescope [2]. This
length l_Q can be initially set from the condition $1/l_Q \simeq$
$K_1(Q)l^*$ that the focal length of the last quadrupole is
equal to the length of the last drift l^*. If the starting value
is too far from l_Q, a thin lens solution might not be reached
for the final telescope.

The aperture of the vertex detector is only used to evalu-
ate the beam collimation requirements from the constraint
that the beam-generated synchrotron radiation must not
impact on it.

3 DESCRIPTION OF THE PROGRAM

FFADA is composed of several modules which are exe-
cuted sequentially. Each one is dedicated to a different
function and generates output and graphics files display-
ing the main results. Some modules needs extra auxiliary
input parameters. We now describe these modules in the
order in which they are executed. A detailed description
of the output and graphics files is given in [8].

3.1 TELE4: analytic derivation of a thin lens solution

This module generates an analytic solution for the 2 tele-
scopes where the last quadrupole of each telescope is a
thick lens as fixed by flc.ffs, and the first 3 are thin
lenses. This solution is obtained by solving, for the given
demagnifications, the 6 dimensional system obtained by
expressing the 6 independent elements of the horizontal
and vertical transfer matrices as functions of the strength
of the 3 thin lenses and the length of the 3 following drifts,
using the solution given in [9]. Once the total length of
the telescopes is known, the CCS optics is scaled to match
the total length of the FFS given in flc.ffs.

Starting from an analytic solution for 2-doublet tele-
scopes where the last quadrupole is already a thick lens,
allows the program to automatically find a solution with
4 thick lenses.

3.2 MAD: 2nd order matching of the FFS and bandwidth calculation

This module calls the MAD program [7] in order to per-
form the following operations:

1. read the thin lens telescope optics generated above
   and the MAD input file ccs.mad describing the optics
   of the CCS;
2. match the optics of the line (MT , CCS , FT) to first
   and second order, with thick elements;
3. plot layout, beta-functions and dispersion;
4. plot the energy dependent beta-functions at the IP;
5. store the matched FFS optics in a MAD file.

The MAD file ccs.mad describing the generic CCS optics
is provided with the program. With some restrictions as
to the coherence of the program, it can be modified and
even replaced by the user to describe another correction
system.

3.3 TRACK: tracking simulations

This module calls MAD to perform tracking simulations of
the FFS. A first simulation is made for 2 bunches of typ-
ically 10,000 particles distributed as defined in flc.beam.
The beam spot sizes and the luminosity from the 2 col-
liding bunches are calculated from the resulting distribu-
tions. A second set of simulations is made to analyze the
energy acceptance of the system. The spot sizes and lu-
minosity are calculated for beams with Gaussian energy
spread varying typically from 0 and 1%. In all cases the
beam-beam forces are neglected.

This tracking module can also be activated with the program DIMAD [10]. However, this requires using a modified version of the DIMAD code in which beam energy profiles $\delta(z)$ can be generated and tracked. With the latest MAD versions (8.14 or later) as well as with DIMAD, the stochastic effect of synchrotron radiation in the magnets is taken into account.

3.4 *DBLT: beam envelopes in the last doublet, collimation and Oide effect*

This module calculates and plots various quantities relevant to the last doublet optics and to the interaction region, namely:

1) the Twiss β and α functions and the beam envelopes from the last doublet down to the IP;

2) the beam collimation requirement arising from clearing the synchrotron radiation generated by the beam in the last doublet, through a vertex detector located at the IP, and through the opposing doublet with hyperbolic or circular aperture. The requirement which minimizes the population of collimated particles, for a uniform distribution of halo, is given and used in the graphics output;

3) the Oide limit [6] for the horizontal and vertical spot sizes at the IP. The calculation is done both analytically and by tracking with MAD (or DIMAD).

3.5 *DIFFLUM: luminosity loss versus beam offset and dispersion at the IP*

For head-on collision, the luminosity is at a maximum with respect to the beam offset, dispersion and coupling at the IP. This module calculates the nominal luminosity expected for head-on collisions and the second order derivatives [11] of the luminosity with respect to the transverse position and angular offsets and dispersions of the *two beams* at the IP. In the calculations, the "hour-glass" effect is taken into account while the pinch effect is not.

3.6 *ERROR: magnet misalignment and field errors, tolerances*

After summarizing the number and types of the magnets included in the system, this module performs a detailed analysis of the effect of small 3d-displacements, 3d-rotations and field errors of the quadrupole and sextupole magnets. These effects are translated to the beam centroid and beam matrix at the IP and analyzed in terms of relative beam offset, dispersion, spot size growth, waist shift and xy-coupling at the IP.

Then, restricting to the 2d-transverse misalignments, the loss of luminosity resulting from uncorrelated random motion of all magnets of the two FFS (except the last doublet) on the one hand, and fixed displacement of the quadrupoles of the two opposing doublets on the other hand, is calculated using the 2nd order derivatives derived in DIFFLUM. This analysis is repeated with the assumption of a perfect steering correction of the beams at the IP.

In the case of no steering, i.e. for uncorrected vibrations, the luminosity reduction arises mainly from the relative beam position offset. In the case where the offset is corrected, the reduction arises from the remaining dispersion, including that introduced by the two opposing steering kickers which are located at the first doublet of the last telescope.

4 FUTURE DEVELOPMENTS

We have presented the first version of the program FFADA. This computer program has been written to facilitate the design, optimization and evolution of final focus systems for linear colliders. It also performs the analysis of the most important properties of the system, such as bandwidth, collimation or tolerances, and then launches tracking simulations of the line. The needed input parameters are meant to be as few and basic as possible. The further developments envisaged are as follows:

1) analyze the effect of misalignment and field errors of the dipole magnets;

2) implement the dependence of the luminosity on the 4×4 transverse phase-space submatrix of the FFS transfer matrix (e.g. include waist-shifts and xy-coupling);

3) derive tolerances on the second and higher order field errors (sextupole and higher multipoles);

4) extend the program to non-zero crossing angle;

5) interface the program with standard or widely distributed graphics software (GKS, HIGZ, TopDraw).

5 REFERENCES

[1] J.J. Murray, K.L. Brown and T. Fieguth, Proc.of Part. Acc. Conf., Washington, D.C., March 1987 & SLAC-PUB-4219 (Feb.1987).

[2] O. Napoly, T.M. Taylor and B. Zotter, Proc.of XIVth HEACC, Tsukuba, Japan (Aug.1989). See also O. Napoly and B. Zotter, CLIC Note 107 (Jan.1990).

[3] R. Helm and J. Irwin, Proc.of 1992 Linear Acc. Conf., Ottawa, Canada (Aug.1992).

[4] R. Brinkmann, "Optimization of a Final Focus System for Large Momentum Bandwidth", DESY-M-90/14 (Nov.1990).

[5] A. A. Sery, "VLEPP Final Focus System", INP Preprint 91-113 (1991).

[6] K. Oide, Phys.Rev.Letters 61,1713 (1988).

[7] H. Grote and F.C. Iselin, "The MAD Program", CERN/SL/90-13 (AP) Rev.3 (Jan.1993).

[8] B.Dunham and O.Napoly, Saclay preprint CEA/DAPNIA/SEA 94-06.

[9] Y-C Chao and J. Irwin, "Solution of a three-thin-lens system with arbitrary transfer properties", SLAC-PUB-5834 (Oct.1992)

[10] R.V. Servranckx, K.L. Brown, L. Schachinger and D. Douglas, "Users Guide to the Program DIMAD", SLAC Report 285 UC-28 (A) (May 1985).

[11] O. Napoly, Part. Acc. 40/4, 181 (1993)

FIELD STABILIZATION IN A SUPERCONDUCTING
CAVITY POWERED IN PULSED MODE

A. Mosnier, J.M. Tessier

Field Stabilization in a Superconducting Cavity Powered in Pulsed Mode

Alban Mosnier, Jean-Michel Tessier

CEA, DSM/DAPNIA/Service d'Etudes d'Accélérateurs

CE-SACLAY,F-91191 Gif/Yvette Cedex, France

Abstract

The Lorentz forces (also called "radiation pressure") and microphonics, by shifting the cavity frequency, are the main bunch-to-bunch energy spread sources. With superconducting cavities operating in pulsed mode, the Lorentz Forces problem arises from the wall deformation response time [1] . The cavity frequency goes on to shift after the field rise time, whereas the beam is passing through the cavity. After a brieve review of the two methods [2,3] coping with the Lorentz forces detuning when one cavity only is fed by one klystron, the effect of parameters spreads is studied when several cavities are fed by one klystron. External feedback loops to minimize the residual amplitude and phase errors are then added and the loop gains are determined. The influence of a spread in external Qs (from coupler tolerances or on purpose for having different fields from cavity to cavity) is analysed and the extra power needed to stabilize the total accelerating voltage is given after an optimization of the beam injection time. Finally, microphonics effects, which can increase dramatically the field errors, are considered and a remedy, allowing to alleviate the problem, is proposed [4].

1. INTRODUCTION

The beam energy spread at the exit the TESLA linac must be below the energy acceptance of the final focus but also small enough to limit the emittance dilution due to chromatic and dispersive effects. The intra-bunch energy spread, resulting from the rf sinusoidal wave and the induced bunch wake potential, can be reduced to about 5.10^{-4}, by running properly the bunch off the crest of the accelerating wave [5]. Any cavity field fluctuation, in phase and in amplitude, during the beam pulse will generate some bunch-to-bunch energy spread. It would be desirable to keep this energy spread below the intra-bunch energy spread in order to assure that the bunch-to-bunch chromatic effects will be no worse than the single bunch ones.

2. DESCRIPTION OF METHODS

During the field rise time, the generator frequency must be locked in any case on the cavity frequency which is shifting because of the Lorentz forces. The phase lock can be provided by a voltage controlled oscillator (VCO) or a self-excited loop. In the first method the generator frequency is then suddenly switched to the reference frequeny (1300 MHz) as soon as the beam is injected into the cavity, leading to a frequency jump at the beam injection time. The secong method uses the self-exciting loop principle during the field rise time and during the beam pulse, without any frequency jump. To minimize the phase shift for both methods during

the beam traversal, the cavity frequency must be higher at the beginning (positive phase slope) and lower (negative phase slope) at the end than the reference frequency. The figure 1 gives the cavity frequency shifts (relative to the reference frequency) and the phase errors evolutions for the TESLA cavity parameters when the initial phase and the initial cavity frequency have been adjusted to cancel the phase deviation when the beam is injected and to minimize the phase error during the beam pulse.
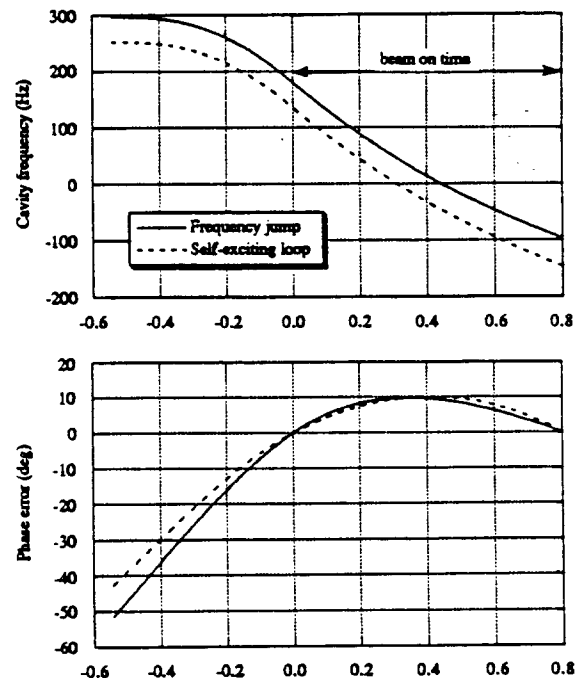

Figure 1 : Relative cavity frequency and phase error for both methods

The TESLA and TTF parameters and the resulting amplitude and phase errors, assuming one cavity driven by one generator, are listed in the table below for comparison.

	TESLA	TTF
Accelerating Gradient	25 MV/m	15 MV/m
Beam current	8 mA	8 mA
electric time constant τ_e	0.78 ms	0.78 ms
mechan. time constant τ_m	1 ms	1 ms
beam injection time $\tau_e ln2$	0.54 ms	0.54 ms
beam pulse duration	0.8 ms	0.8 ms
detuning parameter K	1 Hz/(MV/m)^2	1 Hz/(MV/m)^2
Amplitude error	5-6 10^{-3}	0.7 10^{-3}
Phase error	10 deg	3.5 deg

Without stiffening system, the static Lorentz forces detuning has been estimated to be slightly higher than 1000 Hz for a field gradient of 25 MV/m. With the stiffening system, the detuning reduces to 400 or 600 Hz according to the rigidity of the tuning system. A detuning parameter of 1 $Hz/(MV/m)^2$ has been conservatively retained. The mechanical time constant, which parametrizes the dynamic wall deformation response, has been measured on a 5-cell cavity at 1.5 GHz, and is assumed to be of the same order of magnitude.

3. MEASUREMENTS ON A 1.5 GHZ CAVITY

In order to prove the validity of the methods, they were tested on existing 5-cell cavities at Saclay. Since the Lorentz forces detuning is much stronger on these non-stiffened cavities (a factor 3.6 higher), the same static detuning of about 230 Hz was obtained with a lower accelerating gradient (8 MV/m instead of 15 MV/m). In addition, the beam current was simulated by injecting a rf signal in phase with the beam. The plots 2 show the amplitude and phase errors for the self-exciting loop arrangement during the field rise time and the beam pulse with different initial tunings of the cavity. The phase error was set to zero at the beginning of the beam pulse by readjusting the initial phase for each tuning value. For optimal initial tuning (200 Hz higher than the reference frequency), the amplitude and phase fluctuations are minimum, whereas the amplitude is growing with the time when the cavity is not correctly tuned and the phase slope is positive (negative) just after the field rise time when the tuning frequency is too high (low).
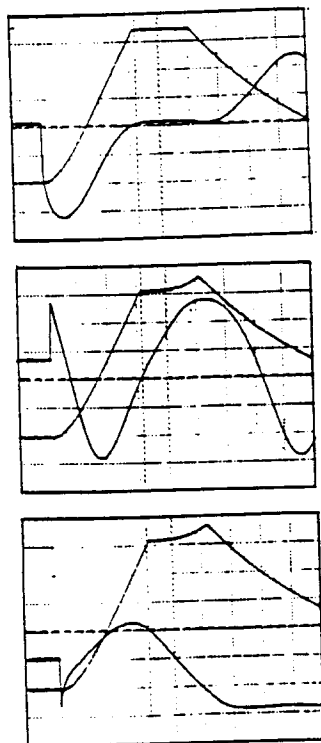
Figure 2 : Measured field amplitude and phase error for optimal (top) too high (center) and too low tunings (bottom) for the self-exciting loop arrangement

4. EFFECTS OF PARAMETERS SPREADS

In the aim to reduce the cost of the power sources, two 8-cavity modules are powered by one 5 MW klystron. Since the rf and mechanical parameters of the cavities are expected to be not identical, the effects of a spread in the different parameters have been studied. During the field rise time, the generator frequency has to be locked on the varying cavity frequency. Since the cavities cannot be initially perfectly tuned, the frequency tracking must be carried out by using the phase signal from the vectorial sum of all cavity voltages and not from a single cavity voltage. With this arrangement, there is no dramatic performance degradation when a spread in the initial cavity tuning or a spread in the detuning parameter K and mechanical time constant are introduced. The figure 3 shows the histograms of the errors for a gradient of 15 MV/m and with 1000 different simulations, where the initial tuning of the 16 cavities has been randomly varied between ± 40 Hz (corresponding to a tuning angle error of 10°).
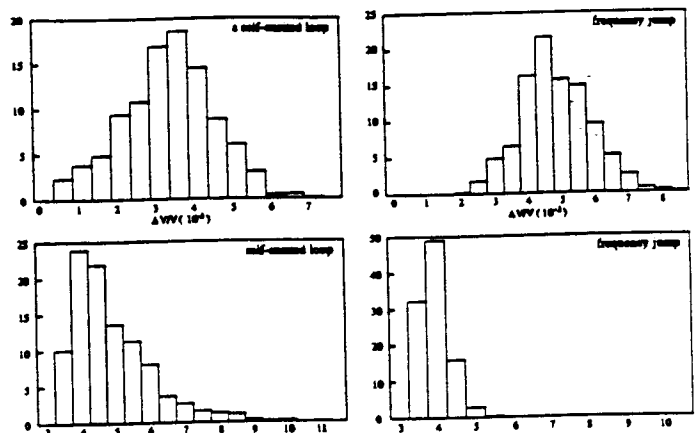

Figure 3 : amplitude (top) and phase (bottom) histograms with static cavity tuning errors for self-excited loop (left) and frequency jump (right) methods

In the same way, the histograms of the errors for a simultaneous spread of 20 % in the detuning parameter K and the mechanical time constant, are showed on the figure 4, for 1000 simulations.
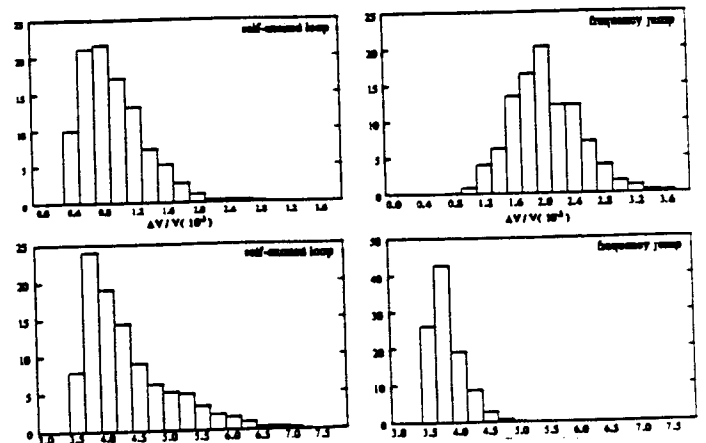

Figure 4: amplitude (top) and phase (bottom) histograms with K and τ_m spreads for self-excited loop (left) and frequency jump (right) methods

5. FEEDBACK LOOPS

Feedback loops have to stabilize the field fluctuations, which are induced mainly either by Lorentz forces or by microphonics detunings, while keeping the needed extra rf power (peak and average) within a reasonable level. In order to reduce the coupling between amplitude and phase feedback, the feedback loops must use a vectoriel modulator, in which an in phase signal, proportional to the amplitude error and an out of phase signal, proportional to the phase error are added to the main drive signal. Loop gains of 50 for the phase and 100 for the amplitude are a good compromise between the extra needed rf power and the resulting amplitude and phase errors. Taking into account the perturbation due to the Lorentz forces only, the resulting energy spread is of the order of 10^{-5} for an increase of the rf powers of about 10% peak and 4 % average.

6. Q-SPREAD EFFECTS

In order to make the best possible use of the SC gradient capability, it would be advantageous to operate each cavity at its maximum field. Since the cavity tuning is not allowed to play with (see previous study), the easiest way of varying the cavity gradients in a chain fed by one klystron, is to change the external Qs from cavity to cavity. Even without Lorentz forces detuning however, a spread in external Qs, resulting from coupler tolerances or on purpose for having different cavity fields, will affect dramatically the amplitude error of the total voltage, because the source is not any more matched to the beam loads. This error must therefore be minimized first by means of the incident power (P_g) and of the beam injection time (t_0), before attempting to close the feedback loops, which would result to a huge extra rf power. Assuming for example a uniform spread in accelerating field around 25 MV/m of a string of 16 cavities, the figure 5 gives the required source power in kW as a function of the total voltage fluctuation for different widths of the gradient spread (10, 15 and 20 %). About 230 kW per cavity (instead of 200 kW) are needed to reach amplitude errors of the order of 10^{-4} for a gradient spread of ± 20 %.
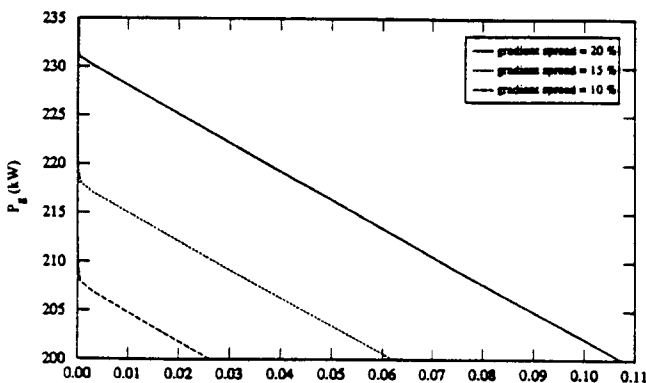

Figure 5: Needed source power (in kW) vs. the fluctuation level of the total voltage

If the Lorentz forces effects are included, the final energy spread is of the order of $2\ 10^{-4}$ with the gains of 100 and 50

for the amplitude and phase loops. The net additional powers to be delivered by the source are finally 30 % peak and and 20 % average with a Q-spread of ± 20 %.

7. MICROPHONICS EFFECTS

The main effect of microphonics, because they change the cavity frequency, is to displace the rf phase with respect to the beam, assuming that the initial phase is fixed. The demand of rf power from the feedback loops would then be huge. Instead of having a fixed initial phase, we could think of a feedback system acting on this initial phase to recover a vanishing phase shift when the beam is coming. Unfortunately the frequencies of mechanical vibrations are expected to be around and above the TESLA repetition rate of 10 Hz, making a direct feedback unefficient. Instead of having fixed phase and amplitude references of the feedback loops, floating references following the actual phase and amplitude at the beginning of the beam pulse (by means of a tracking-and-hold circuits), can solve the microphonics problem in case of too large mechanical vibrations. The beam energy is then constant within a beam pulse but could slightly fluctuate from pulse to pulse. This is not harmful for a long machine like TESLA because the errors coming from the Lorentz forces detuning are correlated whereas the errors coming from the microphonics detuning (jitter) are essentially uncorrelated. The figure 6 shows for example the phase error curves during the beam pulse for 3 cavity tunings, including the Lorentz forces effects : the optimal one and with a shift of ± 50 Hz around due to microphonics, giving moderate extra powers (20% peak and 6% average), with amplitude and phase loop gains of 100 and 50.
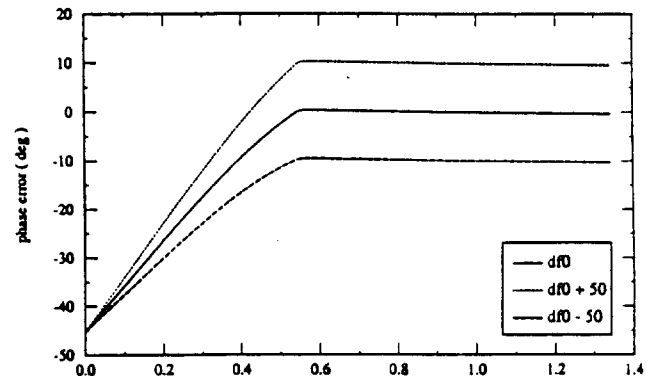

Figure 6: Phase profiles for the optimal initial tuning and ± 50 Hz around

8. REFERENCES

[1] A. Mosnier, "Dynamic measurements of the Lorentz Forces on a MACSE cavity", TESLA Report 93-09

[2] H. Henke, B. Littmann, "Mechanical Parameter Influence on the TESLA Cavity under Lorentz Forces", TESLA Report 93-12

[3] A. Mosnier, "Field Stabilization with Lorentz Forces", DAPNIA/SEA Note 93-03

[4] A. Mosnier and J.-M. Tessier, "Field Stabilization Study for TESLA", DAPNIA/SEA 94-07

[5] A. Mosnier and O. Napoly, "Energy spread Induced in the TESLA Linac", TESLA Report 93-07

BEAM PERFORMANCES OF *MACSE*, THE SACLAY SUPERCONDUCTING TEST ACCELERATOR

M. Jablonka, J.M. Joly, M. Boloré,
J.P. Charrier, B. Dunham, J. Fusellier,
M. Juillard, D. Roudier

Beam performances of MACSE, the Saclay superconducting test accelerator

M. Jablonka, J.M. Joly, M. Boloré, J.P. Charrier, B. Dunham[1], J. Fusellier, M. Juillard, D. Roudier
CEA,DSM/DAPNIA/Service d'Etudes des Accélérateurs
CE SACLAY, F- 91191 Gif/Yvette Cedex, France

Abstract

MACSE is a short superconducting electron linac operated at Saclay[1], to study the problems of acceleration with S.C. cavities. Main beam characteristics like transverse and longitudinal emittances have been measured after the injection line, after the capture cavity and after the main cryomodule. Results are given, discussed and compared to predicted values. Measurement apparatus and methods are described.

1. INTRODUCTION

Over the past 3 years, most of MACSE operationnal time has been devoted to RF experiments with the S.C. cavities, that constituted the main part of its goal. Producing and measuring an electron beam was also, of course, an aspect of the projected experimental program. Beam specifications had been oriented to study the problems of a future machine for nuclear physics : Main nominal parameters are 100 µA and 100% duty cycle. The program of the beam experiments therefore consisted, first to demonstrate the capability of delivering such a beam, in reproducible and stable conditions, then to measure its main characteristics.

2. BEAM MONITORING OVERVIEW

From the beam monitoring point of view, MACSE presents 3 regions : the 100 keV injection beam forming line that precedes the capture cavity; the 2 MeV transfer and analyzing beamline between the capture cavity and the main cryomodule; the high energy (capable of 20 MeV) transport and analyzing beamline. The latter is a long line (~20m), comprising 4 triplets, which transports the beam in a separate room (to avoid radioactivity near the accelerator) where the dipole and the beam dump are located.

These energy variations do not justify different design of the monitoring devices.

For setting up the beam, a pulsed regime has been defined : The pulse length (3 µs) is much shorter than the cavities filling time, so that low level RF loops do not see it, and the repetition rate (25 Hz) is low enough so that the beam can hit any place, as long as necessary, without damage. 25 Hz being half the network frequency, it permits to measure beam parameters free of residual ripple. A synchronous but non 50 Hz submultiple frequency (24.39 Hz) is also available to allow observation of residual ripple at low beam power.

The beam intensity monitoring is performed by toroids transformers. In D.C. beam regime, they still can be used thanks to 3 µs, 3000 Hz "notches" that are made in the beam intensity control signal of the electron gun. These toroids also are in charge of the beam loss monitoring by mean of differential measurement between the begining and the end of the operated beam line.

Beam centering is performed in using viewing screens (made of Cr doped Al_2O3). In the injector beamline, isolated collimators also give a convenient information. At the entrance and the exit of the cryomodules we have installed non isolated collimators that can produce a centering signal thanks to X-ray sensitive photodiodes [2] placed outside the beam tube. This device permitted an ultimate centering of the beam when D.C tests were carried out.

Beam profiles are made with wire scanners that translate an L shaped, 30 µm carbon wire across the beam. They are driven by a stepping motor, at low speed if the pulsed regime is used and at higher speed (40 mm/s) in D.C regime. The control is made through a dedicated VME crate- and the signals can be displayed and interpreted on the screen of the control room work station (Fig 1).

These monitors are installed both on straight beam lines for emittance measurements and on deviated ones for energy spread measurement.

3. D.C BEAM TESTS

We have obtained hours of stable run at 100 µA after careful centering of the beam and also careful setting of the beam loss monitoring and interlocking. One injector collimator had to be redesigned to improve its cooling : We had observed a slow evolution of the intercepted current that was attributed to a local dilatation under the beam impact.
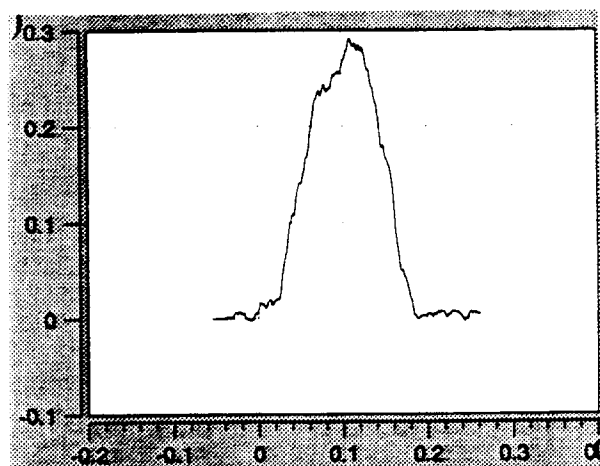

Figure 1 Beam energy spectrum at 12.2 MeV, (σE=7 keV) obtained from a wire scanner (horizontal scale in %)

4. EMITTANCE MEASUREMENTS

In all emittance measurements we have used a multigradient method, i.e. a lens or a triplet force was varied and the beam size measured some distance away in correlation. The calculation then is made in using the method described in [3] when a solenoidal was used (fig. 2). As a D.C. beam could easily burn a hole, only a 40 μA peak, pulsed current has been measured.

Following results give the quantity $4\beta\gamma\varepsilon_{rms}$.

100 keV station : The measurement has been made on the chopped beam. We have found 1.1 π.mm.mrad. The maximum emittance is defined upstream by 2 collimators at 1.3. We can therefore say that the cancellation of transverse deflections by the 2 cavities of the chopping system, following the scheme developped for the NIST micrtron [4] worked quite well.

2 MeV station : We have found an emittance of 2.4 π.mm.mrad, i.e roughly twice the input emittance This is a disappointing result with respect to the 20% maximum increase predicted by Parmela simulations [5]. New and careful measurements should permit to understand this difference that we can for now share between beam misalignment and measurement errors.

High energy station: Measurements have been made with a beam energy of 12.2 MeV. We have found 4.7 π.mm.mrad, i.e., again, a doubling between the input and the output of the 4 cavity cryomodule,.that may have the same causes.

5.ENERGY SPREAD

After the capture cavity, the energy is about 2 MeV. Energy spread (Fig. 2) is optimized by RF phases and amplitudes of the prebunching and capture cavities. Typical measured σE is 7 keV i.e. twice the predicted value.
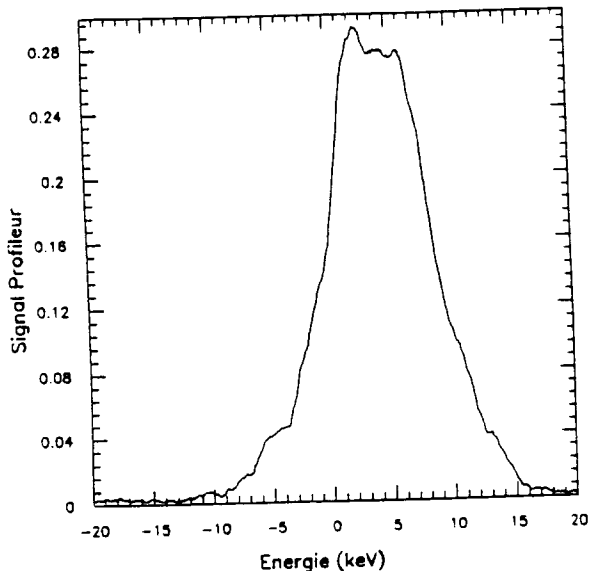
Figure 2 Energy spectrum after the capture cavity. Beam energy is 1.94 MeV. σE=7 keV.

At the high energy station, measurements at 12 MeV, in pulsed regime, for a 40 mA peak current, gave also σE= 7 keV. Increase of energy dispersion due to a finite bunch length is in fact negligible.

6. BUNCH LENGTH

We have not installed any direct bunch length monitor. Instead we have used the very classical "backphasing" method [6]. For the experiment, the 3 first cavities of the main cryomodule (out of 4) were used. The capture cavity and the 2 first cavities accelerated the beam to 8.31 MeV. The 3rd cavity was attenuated to contribute by only 0.46 Mev when phased. Its phase was then shifted by +90° and -90°. Both corresponding energy profiles were recorded. The bunch angular length can then be calculated by :

$$\Theta_{bunch} = \left| \frac{\Delta E_{+90} - \Delta E_{-90}}{2 E_{cav3}} \right|$$

where $\Delta E_{+/-90}$ are the total energy spreads, E_{cav3} is the energy contribution of cavity 3.

We have measured ΔE_{+90}=30.1keV and ΔE_{-90}=10.9keV, hence Θ = 1.2° which is close enough to the expected 1°. The measurement was made very unpractical because of the necessary retuning of the long transport line to the analyzing magnet whenever phases were shifted by a large amount.

7. OTR BEAM PROFILE

Using optical transition radiation for analyzing electron beams profile is a very promissive technique. We have demonstrated its suitability for our low energy, low intensity beam : The radiator was made of a polished stainless steel plate. The pulsed beam frequency was pushed up to 250 Hz. In using a 10^{-4} lux S.I.T. camera, built by Sofretec (France) we have obtained quite satisfactory images. Beam profiles were very conveniently extracted in using the image processing software Laserlab, on a P.C.(fig. 3)
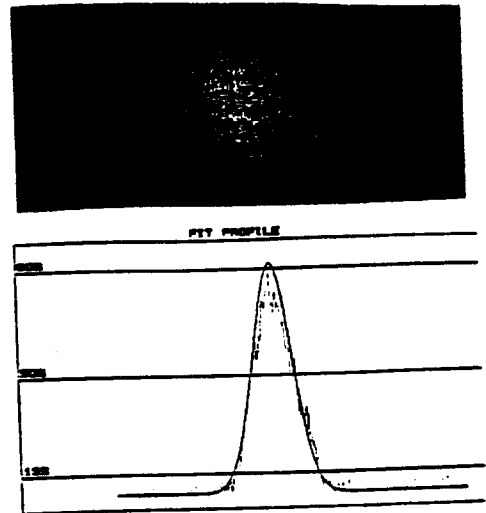

Figure 3 Beam image from optical transition radiation. Below, gaussian fit of the tranverse horizontal profile.

8. NEXT PROGRAM

Our group is now involved in the TESLA collaboration and participates in the construction of TTF (Tesla Test Facility) at DESY. MACSE has permitted to test schemes of pulsed feeding of the cavities under Lorentz forces detuning [7] : A 8 MV/m gradient in a MACSE cavity causes the same relative detuning (with respect to its bandwidth) as will be experienced by the 9-cell TTF cavities at 15 MV/m.

To complete this work, experiments with beam will be soon undertaken : In removing the emittance limiting collimators of the 100 keV line, beam intensity can be raised to 2 mA. 1 ms pulses will be generated. The goal is to reach 100% beam loading, as in TTF design, and to test it.

9. CONCLUSION

Though too few operationnal sessions have been available for these experiments, we conclude that MACSE beam specifications have been achieved. Beam monitors and the computer control system have proven quite a good efficiency. If energy spread and bunch length measurements have been found in sufficient agreement with computer predictions, too a big emittance growth has been observed. MACSE has also proven to be a useful tool for various experiments that were not in its initial program.

8. REFERENCES

[1] "MACSE: Accelerating Electrons at Saclay with Superconducting Cavities", Ph. Leconte, B. Aune et al., Proc. of the 1990 Lin. Acc. Conf..
"First Operation of MACSE the Saclay Pilot Superconducting Electron Linac", B. Aune et al., Proc. of the 1991 P. A. C., 2393.
[2] "Le rayonnement X-gamma dans les cavités supraconductrices", J. Arianer, J. Fusellier, J.M. Joly, G. Lagarde, M. Poitevin, NOTE SFEC T-38, (1989)
[3] "A device for electron gun emittance measurement", B.Aune, M. Jablonka, J.M. Joly, 1985 P.A.C proc., 1896.
[4] "NBS-LANL RTM Injector installation", M.A. Wilson et al., IEEE Trans. Nucl. Sc., NS-30, (1983), 3021.
[5] "The MACSE Injector", B. Aune, M. Jablonka, E. Klein, Proc. of 2nd EPAC (1990), 1246.
[6] "Measurements of the SLAC injector emittance", R.H. Miller, Proc. 1966 Linac Conf., 65.
[7] "Field Stabilization in a Superconducting Cavity Powered in Pulsed Mode", A. Mosnier, J.M. Tessier, These proceedings.

A HIGH CHARGE INJECTOR FOR THE *TESLA* TEST FACILITY

B. Dunham, M. Jablonka

A High Charge Injector for the TESLA Test Facility

B. M. Dunham* and M. Jablonka
DAPNIA/SEA, CE Saclay
91191 Gif/Yvette Cedex, France

Abstract

Several possible models for a high charge injector for the TESLA Test Facility (TTF) have been studied. The injector is required to produce 5×10^{10} e^-/bunch with a pulse length of $\sigma_z = 1$ mm during a macropulse length of 800 μs and a duty cycle of 1%. Two possible schemes are discussed, one starting with a 250 kV thermionic gun and a second starting with a 500 kV DC photocathode gun. The thermionic case requires initial bunching using two subharmonic cavities, while the photocathode gun solution does not. It is demonstrated that a short, normal conducting buncher operating a $\sim$5 MV/m can then efficiently preaccelerate the beam. It is finally accelerated through a 9-cell superconducting capture cavity and compressed to the required bunch length using a chicane-type magnetic buncher. Simulations of the entire injector for both cases show that the needed bunch length can be obtained with a final emittance of ~ 50 π mm mrad.

1 INTRODUCTION

The Tesla Test Facility (TTF), presently under construction at DESY, requires an injector able to produce not only very high charge (5×10^{10} e^-), but also very short bunches ($\sigma_z = 1$ mm). A number of such injectors are already in existence or in the planning stages [2, 3]. Direct application of one of these injectors for the TTF injector would be difficult, however, as TTF requires a requires a long macropulse (1 ms) and a high duty cycle (1%). For this reason a simpler injector (injector #1) has been built first [1], delivering the same macropulse current (8 mA) but in 216 MHz bunches instead of the 1 MHz bunches for the high charge injector. It will consist of a 250 kV gun and a 216 MHz buncher injecting directly into a 9-cell superconducting (SC) cavity powered by a separate 250 kW klystron. The high charge specification will only be achieved by injector #2.

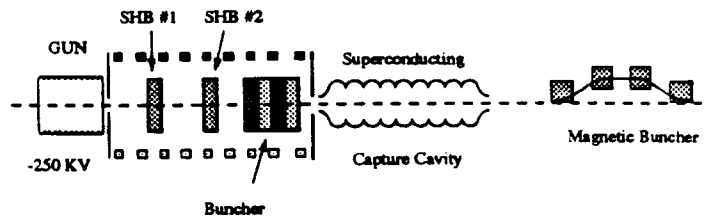*present address: CEBAF, 12000 Jefferson Ave, Newport News, VA 23606

Figure 1: A schematic of the injector model using a thermionic gun.

An RF gun is a possible solution for injector #2, but the required photocathode, laser system and rf cavity would be pushing the limits of the present state of the art due to the high duty cycle and long pulse length. We have proposed to study a conventional scheme, using also a thermoionic gun and 2 subharmonic prebunchers, which is the topic of this paper. A model using a DC photocathode gun has also been studied. Simulations with PARMELA [4] are presented and the use of PARMELA is discussed.

2 INJECTOR MODELS

2.1 Thermionic Gun Model

A schematic diagram of the injector is shown in figure 1. A model for using a thermionic gun was inspired by a design for the NLC injector described by R. Miller [5]. The gun is assumed to operate at 250 kV and emit 5×10^{10} e^- in a rectangular pulse 350 ps wide. A gun with similar properties, 170 kV and 2×10^{10} e^- in 350 ps FWHM (700 ps FW), has been reported [6]. Initial bunching is performed by two 650 MHz subharmonic bunchers (separated by $\sim$50 cm).

For high charge injectors it is necessary to immerse the beam (from the gun on) in a continuous solenoidal field to counteract the huge space charge forces. As this is not possible to do with a SC capture cavity, it is proposed to pre-accelerate and bunch the beam using a 4-cell, $\beta = 1$ normal conducting (NC) buncher. Assuming a shunt impedance of 50 MΩ/m and a total length of $\sim$50 cm, 250 kW of power is required to ob-
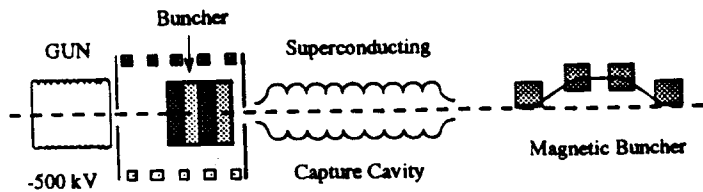
Figure 2: A schematic of the injector model using a photocathode gun.

tain an accelerating field of 5 MV/m. This is the same value as is required to power the SC capture cavity for the low charge injector for TTF, so an identical klystron and modulator could be used. This buncher is located 25 cm after the second subharmonic cavity.

After the NC buncher, it is planned to use the 9-cell SC capture cavity of the low charge injector to boost the beam energy. The distance between the NC and SC cavities should be as short as possible, and the length surrounded by a solenoidal field. To obtain the desired final bunch length, the accelerated beam is further compressed using a chicane-type magnetic buncher (MB).

A basic chicane-type magnetic buncher is a relatively simple achromatic system, requiring only four identical rectangular bending magnets. The path length variation of the MB can be adjusted by changing the bend angle to match the phase-energy correlation of the beam from the RF bunching system. The MB in these simulations uses dipole magnets 15 cm long with bend angles of $\sim 30°$ for an overall length of $\sim$1.2 m and a resulting $R_{56} = -.17$ cm/%.

2.2 Photocathode Gun Model

Figure 2 shows an alternative model using a high-voltage DC photocathode gun as an electron source. This is not exactly an off-the-shelf item, but it has properties which are interesting enough to warrant an investigation. Such a gun is now under construction at CEBAF [7] for use as an injector for their FEL project, and is designed to produce 0.12 nC, 100 ps bunches at 500 keV using a GaAs photocathode. Simulations show [8] that it is capable of producing the 8 nC bunches needed here with an emittance of 30 π (all emittances are normalized, rms values with units of mm–mr) and a beam radius (diverging) of 2.6 cm.

The ability to generate 100 ps bunches obviates the need for subharmonic bunching, and allows direct injection into the NC capture section. This feature makes the injector much more compact and reduces the number of components in the beamline. In addi-

tion, since the gun needs only a 500 kV DC power supply (commercially available) for operation, a complicated and space consuming modulator is not required. Some disadvantages are the need for semiconductor photocathode processing techniques, as well as an expensive laser system.

3 BEAM DYNAMICS

3.1 Introduction

The space charge forces on the macroparticles in PARMELA are calculated in the usual fashion by superimposing a 2-D cylindrically symmetric mesh over the particle distribution in the rest frame of the bunch and determining the fields due to the particles in the bins. This method has the advantage of running quickly, but there are many free parameters to set so one must carefully check output variations with changes in these parameters.

Since the bunch length changes dramatically during the bunching process, it is important to vary the total mesh length in the longitudinal direction as the bunch compresses. We have introduced a routine in PARMELA to automatically do this. Using this adaptive meshing method gives convergent results for the final emittance using the smallest number of bins (25) compared to requiring over 50 bins for convergence when the initial mesh length is not varied (see [9] for complete details of this and of all the simulations described in this report). This is important to know as one wants to use as few bins as possible in order to speed up execution. The meshing in the radial direction is not as important as the radial beam dimensions do not vary so dramatically.

In these simulations, PARMELA hard edge solenoids are used to model the magnetic field along the beamline and the subharmonic bunchers are represented using a zero-length, ideal buncher with a sinusoidal field. The normal-conducting buncher is described using the internal field values provided in PARMELA for a 1300 MHz Los Alamos side-coupled structure. The accelerating field for the entire 9-cell SC cavity is calculated using URMEL and a Fourier transform of the fields is included in a separate subroutine.

3.2 Thermionic Model Results

Figure 3 shows the radial and phase variation and emittance growth of the beam for the thermoionic injector model. The bunch is compressed by a factor of ~ 30 to reach a final bunch length of $\sigma_z = 1.4°$
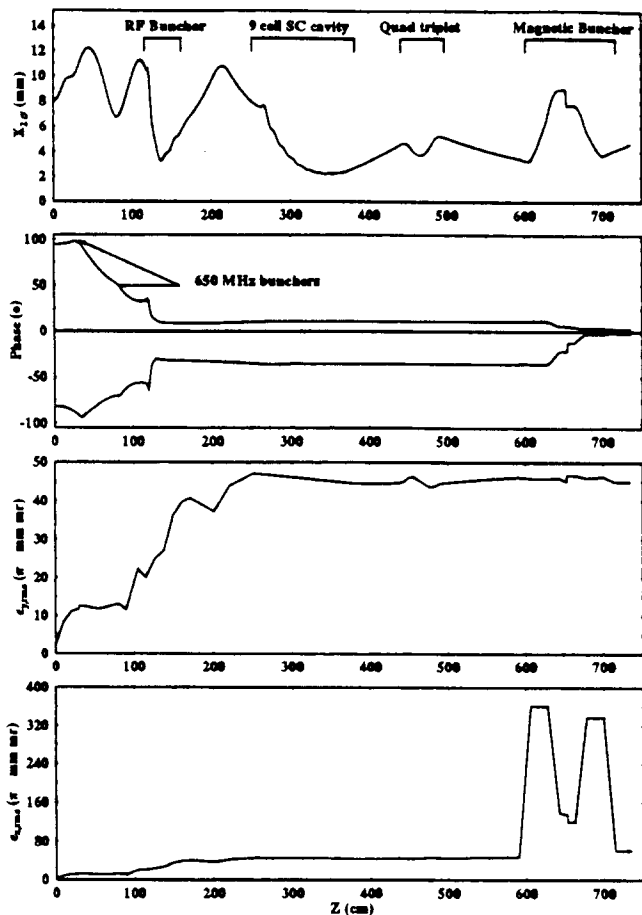
Figure 3: The top figure shows the 2-σ beam envelop for the horizontal plane and the second figure shows the phase compression envelop. The bottom two figures show the emittance growth in the vertical and horizontal planes.

at an energy of 16 MeV. The emittance grows by a factor of 12 to 45 π in the vertical plane, and to 65 π in the horizontal plane after passing through the MB. Without space charge the horizontal emittance explodes in the bending region, but cancels out at the end of the achromatic magnetic buncher system. With space charge the dispersion is no longer suppressed and a net emittance growth results. All of the parameters were optimized to keep the emittance growth as small as possible while obtaining a good phase compression.

3.3 Photocathode Gun Model Results

The plots for the photocathode gun model are similar to those for the thermionic model and are not shown here (see [9]). In this case, it was possible to reach a final bunch length $\sigma_z = 2.2°$ without using a MB by phasing both the NC buncher and the SC cavity off crest. The resulting emittance is high (75 π),

though, and the energy is low (13 MeV). By varying the phases, it is possible to obtain a beam with an energy of 16 MeV and an emittance of 60 π, but a MB is required.

4 CONCLUSION

From the simulations performed here, one can conclude that an injector can be built that will fulfill the requirements for a high charge injector for the TESLA Test Facility. Such an injector would consist of an electron gun (either thermionic of photocathode), two subharmonic bunchers (not necessary for the photocathode gun), a 4-cell, normal conducting buncher, a 9-cell superconducting structure, and a magnetic buncher. The exact details of the models depend very strongly on the actual properties of the electron gun to be used. For future simulations, the model should include the measured parameters of an existing gun, as well as more realistic characterizations of the the elements of the injector. Effects such as wakefields, beam loading, and instabilities have not been included.

5 REFERENCES

[1] "The TESLA Test Facility Linac Injector", these conference proceedings.

[2] A. Yeremian *et al.*, Proc. 1989 Particle Accelerator Conference, 657 (1989).

[3] S. Takeda *et al.*, IEEE Trans. Nucl. Sci., **NS-32**, 3219 (1985).

[4] K. Crandall and L. Young, private communication.

[5] R.H. Miller, presented at the TESLA collaboration meeting, Fermilab, 1993.

[6] H. Matsumoto *et al.*, Proc. 1992 Linear Accelerator Conference, 296 (1992).

[7] C.K. Sinclair, Nucl. Instr. and Meth. **A318**, 410 (1992).

[8] D. Engwall, private communication.

[9] B.M. Dunham and M. Jablonka, Technical Note CE-Saclay, DAPNIA/SEA 94-05.

THERMAL TESTS OF *HOM* COUPLERS FOR
SUPERCONDUCTING CAVITIES

S. Chel, A. Mosnier, M. Fouaidy,
T. Junquera

Thermal Tests of HOM Couplers for Superconducting Cavities

S.Chel, A.Mosnier

CEA,DSM/DAPNIA/Service d'Etudes d'Accélérateurs
CE-Saclay, F-91191 Gif-sur-Yvette, France

M.Fouaidy, T.Junquera
Institut de Physique Nucléaire (CNRS-IN2P3)
F-91406 Orsay, France

Abstract

In order to restrict the multi-bunch phenomena due to long-range wakefields in the TESLA linac, the higher order modes of the cavity must be damped down to the 10^4-10^5 level. For this purpose, HOM-couplers, mounted at both ends of the cavity, must couple strongly to the most dangerous modes, while rejecting by means of a filter the accelerating mode. Two versions have been developed [1], one is welded to the beam tube and the other one is demountable thanks to an intermediate flange. In this paper, we present the results of high power tests performed on the demountable version with a special test stand, including a single-cell cavity, a 5kW klystron and the coupler itself, as well as thermal simulations, which were initiated previously [2] with the help of a finite elements code. Accelerating field of 21 MV/m in cw mode, limited by cavity quenches and not by the coupler, was achieved, giving a confortable safety margin if one keeps in mind that the duty cycle of the TESLA pulsed mode is lower than 2 %. Moreover, by intentional detuning of the filter, the coupler was capable to transmit a peak power of 1.75 kW for the TESLA beam pulse duration, higher than the maximum HOM power which could be resonantly excited by the beam.

1. INTRODUCTION

The key component of the demountable coupler is a loop whose plane is orthogonal to the beam axis (see figure 1), which couples mainly to magnetic field for the dipole modes and mainly to electrical field for the longitudinal modes. The rejection filter of the fundamental mode is simply formed by the inductance of the loop itself and the capacity between the loop end and the outer conductor [3]. No stringent fabrication tolerances are required and the final tuning of the filter can be performed outside the clean room, once the coupler is mounted and the cavity is closed, with the help of the small bellow located above the Helicoflex gasket. The present design of the LHe-vessel of the TESLA cavity prevents from a direct cooling of the coupler by LHe. The loop is then simply cooled by conduction through the upper stub, which can be however linked to the LHe bath through a thermal shunt. Since the integrated filter has to a sustain very high reactive power (the external Q of the coupler without filter with respect to the accelerating mode is only a few 10^6), the thermal behaviour of the device under high RF power must be carefully studied. We present and discuss the results of RF tests and calculations obtained with different couplers mounted

on the beam tube, which was not in direct contact with the LHe bath, of a single-cell cavity.
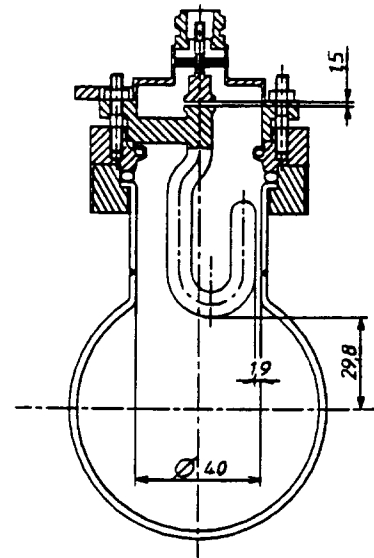

Fig. 1 : Drawing of the demountable HOM coupler

2. TEST STAND AND CALIBRATION

For the power tests, we used the existing 1497 MHz RF equipment. The cavity and coupler dimensions were then scaled from the 1300 MHz TESLA frequency to 1497 MHz. However, in order to push away limitations due to cavity quenches, the coupling of the scaled version to the accelerating mode was made on purpose five times higher than the final 1300 MHz TESLA version. The distance between the cavity iris and the HOM coupler was decreased, while the loop penetration in the beam tube was increased. With this test arrangement, the surface magnetic field at the filter location is about 3 Gauss/MV/m. We also used calibrated thermometers fixed around the coupler and the beam tube for temperature measurements. On the other hand, the important parameters which can be only deduced from experimental data, such as the thermal contact resistance at the sealings, were determined by means of a special arrangement using a heater. This arrangement looks like the real coupler (Fig. 2) and was also used to check the thermal simulations. A manganin wire heater, attached to the end of the loop, is used to simulate the RF losses and the resulting temperature distribution around the coupler and the uncooled beam tube is measured as function of the heater power (Pheater).
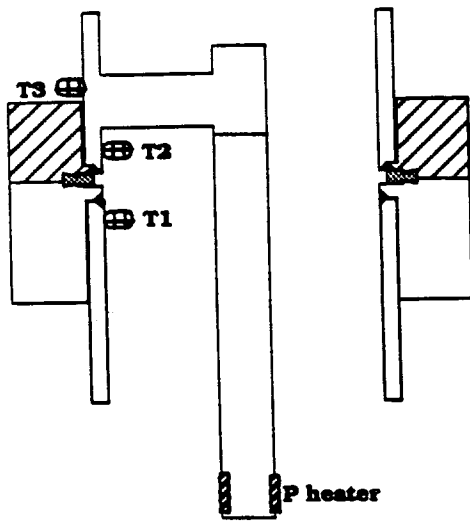
Fig. 2 : calibration test assembly

The results showed an important thermal contact resistance across the flanges. An overall equivalent thermal conductivity k_{eq} to this assembly can then be defined by :

$$\int_{T_i}^{T_3} k_{eq}(T)\,dT = P_{heater}\,\frac{L}{S}$$

where L and S are geometrical parameters. The value of this equivalent thermal conductivity at 4.2K is 720 times lower than that of the Nb used for the tests (RRR=270).

Furthermore, by introducing k_{eq} in the simulation model, the resulting temperature distribution is very close to the measured values (Fig. 3). Moreover, the Nb critical temperature is reached at the extremity of the inner conductor for a heater power of 60mW inducing a temperature difference across the flanges of 6.2K.
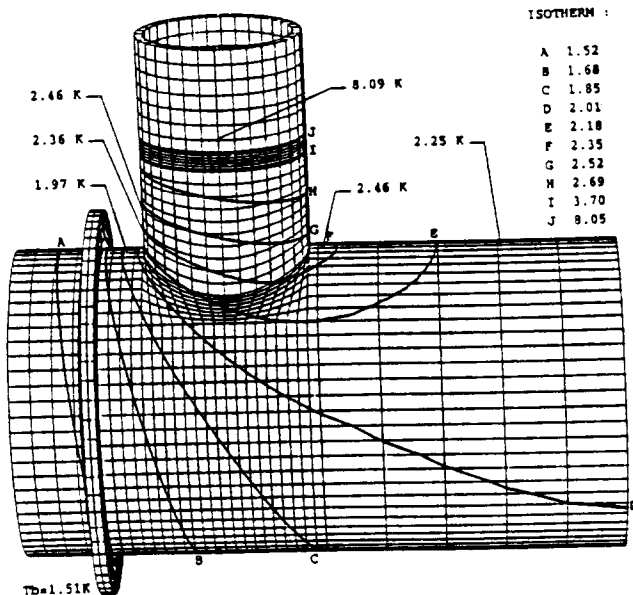
Fig. 3 : measured and computed temperature distributions for a heater power of 46mW

Consequently the thermal breakdown of the coupler will be mainly controlled by this thermal contact resistance, and only a small gain on power capability (<10%) is obtained by using a loop made of sputtered niobium onto a copper substrate.

3.   RESULTS OF THE RF TESTS

A. Without thermal shunt

Preliminary tests were performed without any thermal shunt in cw mode. Various configurations were used : different loop geometries (cylindrical and bean shaped capacitor), different construction materials (bulk Nb, Nb/Cu) and/or different tunings ($2.10^{10} < Qex_{fund.} < 6.10^{12}$). For all these tests, the quench of the coupler occured for cw accelerating fields in the range 11-14 MV/m and was always characterized by the same phenomena (Fig. 4) : Eacc jumps from the maximum field to ~2MV/m at the same incident power, the quality factor drops from ~10^{10} to ~10^9, the $Qex_{fund.}$ of the coupler decreases by ~30%, the maximum temperature measured during the RF test reaches values higher than 20K.

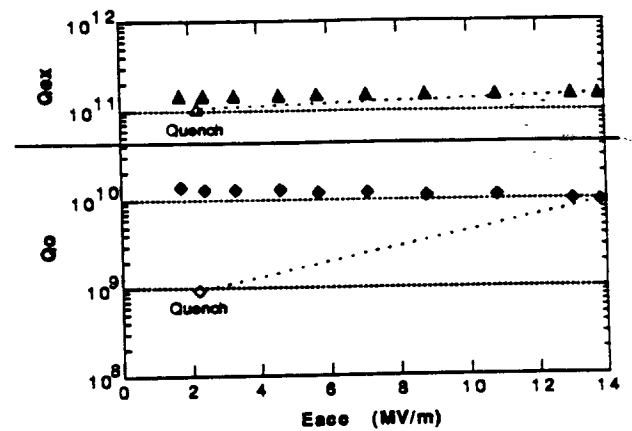
Fig. 4 : Qo and Qex versus Eacc for a Nb HOM coupler without thermal shunt.
(Solid symbols : values before the coupler quench
Open symbols : values after the coupler quench).

From the test corresponding to Fig. 4, it is possible to evaluate the dissipated power of the HOM after the quench. Before the quench at a field of 2.1 MV/m the Qo value gives a dissipated power in the cavity of 31mW (all the other dissipations are neglected at this very low field). After the quench of the HOM coupler and for the same field, the Qo value is about ten times lower, leading to a dissipated power in the coupler of 430mW. The dissipating area is the region where the magnetic field is highest, i.e. the extremity of the loop. At this location, from the dissipated power and the value of the magnetic field, one can deduce a surface resistance of $5.3m\Omega$ which is consistent with the measured temperature of 26K. Once the quench of the coupler is reached (Tmax ~ 25K), about 3 minutes are needed for recovering the s.c. state with a maximum temperature lower than 4K. It is worthwhile noting that even without thermal shunt, the quench of the coupler, which occurs at 14 MV/m in cw mode, will occur at a much higher field for the TESLA pulsed mode (2% d.c.). For example, the thermal breakdown was observed at 20.7 MV/m for a duty cycle of 40 %. However, since the coupler could be

exposed to intense field conditions if the cavity has to be processed in-situ with pulsed peak power, and in order to increase the safety margin in normal operation, a thermal shunt linking the upper stub to the LHe-vessel was added.

B. With thermal shunt

In order to by-pass the gasket, the stub of the HOM coupler was connected to the LHe tank by a thermal shunt (standard braided copper wires). The test with this arrangement was limited by a quench of the cavity at 21 MV/m, but up to this value the coupler did not show any anormal behaviour (Fig. 5).
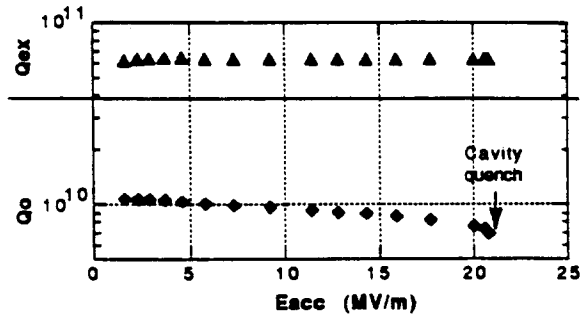
Fig. 5 : Qo=f(Eacc) (Nb HOM with thermal shunt)

With a LHe bath temperature of 1.65K, the maximum temperature measured around the coupler (Fig. 6) is 4.06 K at the maximum field level. A test in pulsed mode with 18.6% duty cycle at the same field level (21 MV/m) showed oscillations of the maximum temperature between 1.94K and 2.22K, consistent with the curve of Fig. 6 obtained in cw mode if one considers the average squared field ($= E_{acc}^2 \cdot d.c.$). Using the calibration test assembly, the heater power needed to reach the Nb critical temperature was 285mW (as compared to 60mW without the thermal shunt).
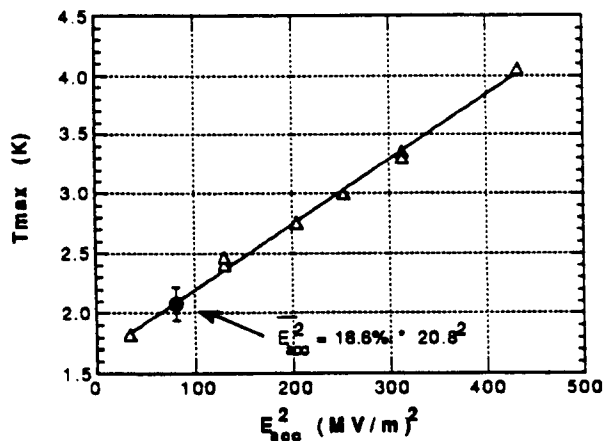
Fig. 6 : Maximum temperature measured in cw mode (triangles) and in pulsed mode (dot).
(Linear fit : $T_{max} = 1.65 + 5.47\,10^{-3}\,E_{acc}^2$)

In addition, the coupler was tested with the TESLA beam pulse (10Hz, 0.8ms) and a detuned filter to simulate the peak power which could be induced by resonantly excited HOMs. A peak power of 1.75 kW, higher than the expected HOM power

which could be extracted in the worst case, was transmitted before reaching the anormal heating of the coupler. The hotest point during this test was located close to the N-SMA transition at the RF output of the coupler.

4. MULTIPACTOR AND FIELD EMISSION

No multipactor was detected with the final coupler whose filter capacitor is made of the end of the straight cylindrical inner conductor and the outer conductor. However, the multipactor was clearly identified with a coupler whose capacitor IC is bean shaped. Taking into account the capacitor gap variation due to a concentricity default between the bean shaped IC and the outer conductor, multipactor is expected to occur theoretically in the Eacc range 1.6-2.2MV/m. This is consistent with our observations among which : the high temperature values for Eacc = 1.8MV/m, the random strong and fast temperature increases in the vicinity of the capacitor during the field rise or fall of some pulses for 13.2MV/m (the maximum temperature is measured at this location while it is measured in front of the stub without multipactor), and the electronic current measured at the RF output of the coupler.

For each test, the computed and measured temperature distributions are in good agreement for all the thermometers excepted those located on the uncooled beam tube (systematically higher than the computed values by 0.3 K to 1.0K depending on Eacc). The emitted electrons from the cavity could dissipate a power of up to 1 W on the beam tube if we assume typical values for the involved parameters (electron kinetic energy, e⁻ current, ...). This additional heat load could explain the observed discrepancy.

5. CONCLUSION

The thermal behaviour of the demountable coupler has been still enhanced thanks to a thermal shunt. A cw accelerating field of 21 MV/m, limited by a cavity quench, was then reached. The maximum temperature measured in front of the stub is 4.0 K at this field level, and decreases to 2.1 K with a duty cycle of 18.6 %. The coupler should then operate with an important safety margin with TESLA parameters (1.4% d.c. and 25 MV/m). Moreover, the test with a detuned filter and the TESLA beam pulse showed that the coupler could handle a RF power of 1.75kW, higher than the maximum power extracted from HOMs when they are resonantly excited by the beam.

6. REFERENCES

[1] Sekutowitcz, "HOM coupler for TESLA ", 6th Workshop on RF Suprconductivity, CEBAF, 1993

[2] M. Fouaidy et al., "Thermal study of HOM couplers for s.c. RF cavities". IEEE Part. Acc. Conf., Washington D.C., 05/1993.

[3] A. Mosnier, "Developments of HOM couplers for superconducting cavities", 4th Workshop on RF Superconductivity, Tsukuba, 1989.

STATUS AND APPLICATION OF SUPERCONDUCTING CAVITIES

B. Bonin

Status and applications of superconducting cavities

B. Bonin

CEA DAPNIA SEA

Saclay F-91191 Gif sur Yvette, France

Abstract

This paper sketches the most recent trends of the R&D and applications of RF superconductivity to accelerators.

1. INTRODUCTION

Superconducting cavities have now been used in many accelerators, eg heavy ion linacs, large storage rings at CERN, KEK and DESY, electron linacs at Stanford, Darmstadt, Saclay-Orsay and CEBAF, or free electron laser drivers. Experience gained during the building of these machines strongly suggests that RF superconductivity is already a mature technology, even if it is still far from its limits. New applications are now being envisaged, both at the high luminosity and at the high energy frontiers of the accelerator technology.

The physics and accelerator applications of RF superconductivity have been excellently reviewed by many authors [1-5]. The present paper will concentrate only on the highlights and on the most recent developments in the field. Included topics are large scale fabrication, thin films, surface preparation and cavity performance level. Despite its importance and its close connection to cavities, the problem of RF couplers and windows has been deliberately omitted in this article. The most important issues of the R&D on superconducting cavities, ie the quest for high gradients and reduced RF dissipation, will be reviewed.

2. HIGH GRADIENTS

The accelerating gradients available in accelerating superconducting structures have been in considerable progress recently, increasing by as much as 50% during the last two years. This progress may be ascribed to the conjunction of at least four factors: improved cleanliness standards [6], the development of RF processing techniques like High Peak Power Processing [7-9], the availability of higher purity niobium [10], and the generalization of the heat treatment of the cavities [11,12].

Accelerating gradients are still limited by two phenomena: quenches and field emission. The impression gathered from a systematic compilation of the results worldwide is that roughly 50% of the gradient limitations are due to quenches, while the remaining 50% come from electron emission.

The maximum electric field that can be obtained without field emission depends on the area exposed to the field. Surface fields higher than 100 MV/m have been obtained without electron emission on areas of the order of 1 cm^2 [13]; superconducting radio-frequency quadrupoles

(RFQ) have reached a peak electric field of 128 MV/m [14]; surface fields of 50 MV/m have been reached often at about 1 GHz on single cell accelerating cavities, and 35 MV/m on 3- or 5-cell cavities. The largest data base comes from CEBAF (5 cell, 1.5 GHz, T = 2K), [15], (fig. 1). The results are very encouraging, since nearly all the CEBAF cavities tested so far exceed by large amounts the design value: the average surface field obtained is close to 20 MV/m. Moreover, there is no significant degradation of usable gradient of the CEBAF cavities between their test in a vertical cryostat and their use in the accelerator. Similar gradients have been achieved in a much smaller test series on 9-cell cavities at Cornell and Wuppertal (3 GHz, 1.8 K). There is much confidence that surface fields as high as 30 MV/m can be obtained reliably, without electron emission, in 9-cell structures at 1.3 GHz. With the ratio $E_{surface}/E_{acc} = 2$ currently obtained in present day "$\beta=1$" cavity designs, this corresponds to accelerating gradients of 15 MV/m.
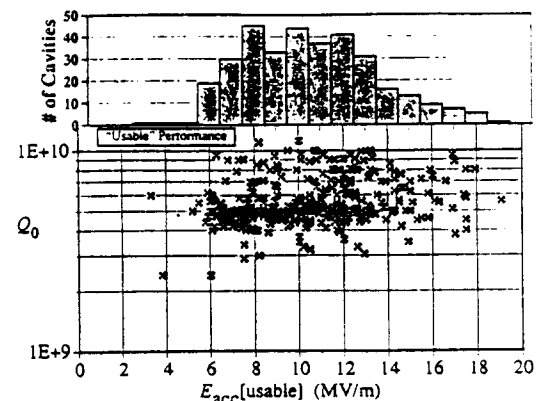

Figure 1 Systematics of the 1.5 GHz, 5-cell cavities from CEBAF (from ref. 15).

2.1 Field emission

It is now recognized that field emission in cavities is due to surface defects of micrometer size, causing electron emission from the surface and subsequent loading of the cavity [16]. Recent systematic studies have confirmed that deliberate contamination of the cavity surface by conducting, micrometer sized particles results in heavy field emission [17]. Insulating particles seem to be much less dangerous. The relevance of this information for the case of SC cavities may be discussed, but a rigorous cleanliness of the cavity surface seems to be an indispensable prerequisite to avoid field emission. So far, efforts have concentrated on the prevention of particulate contamination during the chemical treatment of the cavity,

and during the subsequent rinsings. Among the advanced cleaning techniques presently under investigation, high pressure rinsing seems to be most promising [18,19]. Its idea is to use the mechanical action of a high speed water jet to remove micron sized particles adhering on the surface.

Particulate contamination also arises during assembly and pumping of the cavities. The assembly steps involve unavoidable contact and abrasion of metal parts, liable to generate metallic dust particles and field emission. Despite its considerable potential of improvement, this problem has received much less systematic attention than the problem of cleanliness during the wet process.

2.2 RF processing

High peak power processing (HPP) is another possible recipe for suppressing field emission in superconducting cavities. It consists basically in sending a RF pulse intense enough to "burn" the electron emitters, during a time short enough to prevent a quench [7–9]. A two-cell, 3 GHz cavity reached a maximum surface field of 100 MV/m at Cornell after such a high peak power processing. This is certainly a very promising technique, but its applicability to the real case of an accelerator is not demonstrated yet. If HPP is to be applied on a cavity already installed in an accelerator, the coupling line will have to withstand the power necessary for the treatment (of the order of 1 MW/m). This requirement cannot be met in most accelerators. However, "moderate power processing" (a few kW/m) is much more readily applicable in situ, has proven its validity [20], and is used, for example at CEBAF and on MACSE. On the other hand, the usefulness of HPP as an "ex situ" treatment is not yet fully established, because it remains to be seen to what extent the benefit of the treatment is kept after a dismounting of the cavity and a new exposure to air.

2.3 Quenches, and the problem of niobium purity

The limitation of gradients by quenches (ie thermal instabilities of the cavity initiated by heating defects) has been a severe one in the past. Improved fabrication techniques and the use of high purity niobium already restrict the occurrence of quenches to about 20% for Nb single cell accelerating cavities in the GHz range with gradients smaller than 15 MV/m. High temperature vacuum annealing of the cavity gives the possibility of increasing the wall thermal conductivity, and the cavity quench threshold. It is striking to see that in all laboratories, the highest gradients have been obtained with fired cavities. For example, accelerating gradients as high as 30 MV/m have been reached at Cornell on single cell cavities at 1.5 GHz after heating the cavity to 1300°–1500° C (fig. 2). Unfortunately, the heat treatment has many drawbacks: it is expensive and difficult to integrate in a large scale production process. Moreover, it severely degrades the mechanical properties of the cavities. Despite these shortcomings, heat treatment seems to be an obliged detour on the road to high gradients.
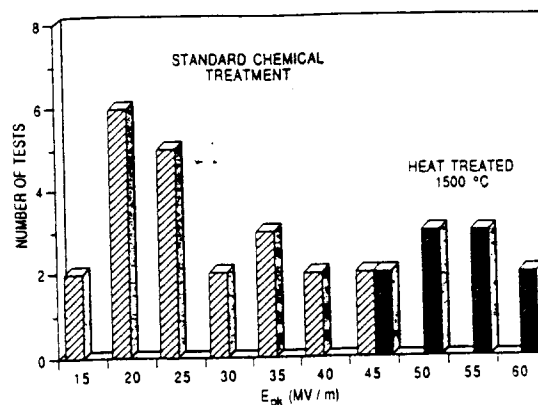

Figure 2 Benefits of the heat treatment on single cell niobium cavities at Cornell (from ref. 1).

A significant proportion of the CEBAF cavities are still limited by quenches. This probably means that the cavity chemical treatment and handling are done in very clean conditions, thus preventing field emission. Another consequence is that these cavities might reach higher gradients after a purification improving their thermal conductivity. Definitely, a niobium purity of RRR 200, which has been the "state of the art" during the last five years, is not sufficient for high gradient applications!

In the far future, it is probable that the purification of Niobium will be achieved at the stage of the Nb sheet production. A high purity Nb sheet of RRR 350 with adequate formability can already be ordered from industry. Prospects of further improvement are good, since very high purity Niobium (RRR > 600) is in principle available from russian industry [21]. However, it is known that the forming of niobium sheet introduces a large density of dislocations in the material, thereby reducing its RRR and thermal conductivity. This might reduce somewhat the advantage of using very high purity Nb sheet as a starting material. This problem has been largely overlooked in the past, due to the difficulty of measuring the RRR of a cavity already formed into shape. In this context, heat treatment of the material at the stage of the half cell production remains an interesting option.

3. PROGRESS IN Q-VALUE

It is essential for the success of many kinds of superconducting accelerators to minimize the RF power dissipated in the cavities. Substantial progress has been made during the past two years. The main cause of non-reproducibility of the cavity Q value, i.e. hydrogen contamination, has been understood [22] and eradicated to a large extent. In all laboratories, this effort yielded cavities with reproducible residual surface resistance, between 10 and 20 nΩ. Surface resistance as low as a few nΩ have indeed been observed, for example at Wuppertal ([23], fig. 3) or at Saclay. This corresponds to $Q_{res} = 5$–$6 \ 10^{10}$, a value now routinely obtained in vertical test cryostat at Saclay, even with non heat-treated accelerating cavities. This result, obtained thanks to an especially careful magnetic shielding of the cavities, and a minimization of the losses in the cutoff tubes, has considerably clarified

the list of possible causes of residual dissipation in super-conducting cavities. Putting aside the two major causes already mentioned, this list featured [24] dielectric losses in the Nb_2O_5 oxide layer and in the adsorbed species, normal conducting inclusions, oxide-induced surface ser-rations, geometrical defects like cracks, crevices or de-laminations, losses in the disordered layer at the Nb-oxide interface, losses in the grain boundaries,....... The order of magnitude of each contribution was poorly known : we now know from experiment that their sum amounts to less than a few $n\Omega$ for state-of-the art, non heat-treated cavities. This value can and should become a standard for vertically tested cavities. It remains to be seen to what extent the benefits of this improvement in Q value are kept in a real accelerator environment, where the de-mands on magnetic shielding, cavity design, and cooling speed are met less easily. If significant improvement in Q values can be obtained in real accelerators, the cost of CW accelerators could be reduced by reduction of the needed cryogenic power. This might also permit opera-tion of pulsed accelerators like TESLA with duty cycles larger than the ones envisaged now.
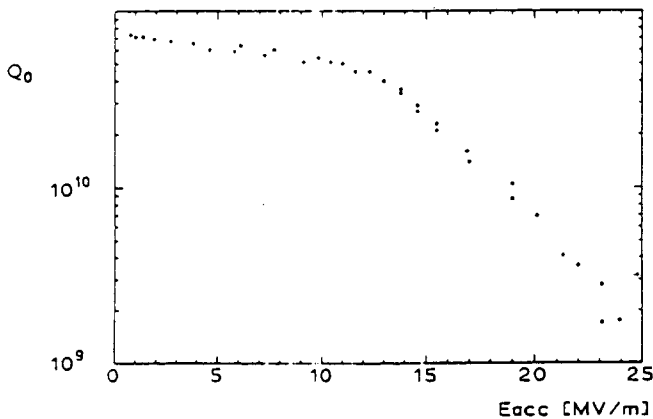

Figure 3 Very high Q-value obtained in a 3 GHz single-cell niobium cavity at Wuppertal (from ref. 23).

4. CAVITY FABRICATION

In most cases, low-beta structures are produced in limited number. Their fabrication poses problems which can be solved at the laboratory level. The situation is very different for $\beta=1$ cavities, which are often to be produced in large quantities for a given accelerator project. Here, the fabrication cost and quality of the product become industrial problems.

Presently, most $\beta=1$ accelerating cavities are made from Nb sheet, and their fabrication includes forming of half cells from sheet material, and electron beam weld-ing of the half cells. This "EB welding method" is very delicate because of the requirements it imposes on the de-gree of cleanliness of the surfaces to be welded. It is also time consuming and poorly suited to large scale produc-tion in industry. It involves many operations, especially

for cavities with a large number of cells. Besides, even with a good vacuum in the EB welder, the preservation of the niobium purity at the welds becomes increasingly difficult to guarantee, if very high purity niobium is used.

Alternative approaches based either on spinning a single niobium sheet [26] or hydroforming a tube [27] to produce seamless cavities are under investigation. The drawability of niobium seems to be sufficient for this pur-pose, but forming of refractory metals is a very delicate process, especially if high purity material is used. These new methods will probably involve intermediate anneal-ings of the cavity during fabrication. It remains to be seen whether the number of annealings and the purity of the material can be maintained at an acceptable level. In case of success, these techniques might result in a very signifi-cant reduction of costs for a large scale cavity production.

4.1 Thin superconducting films

In RF superconducting structures, the superconduct-ing current flows in a very shallow skin depth, of the order of 100 nm. This suggests the use of a thin superconduct-ing film deposited inside the cavity. The expected gain is threefold: a metal with good thermal conductivity can be chosen as substrate, with a subsequent enhancement of the cavity thermal stability ; the substrate (eg OFHC copper) is cheaper than niobium sheet ; the thin film may have improved superconducting properties as compared to niobium. Investigations have been made mainly with Nb, NbN, NbTiN and Nb_3Sn thin films.
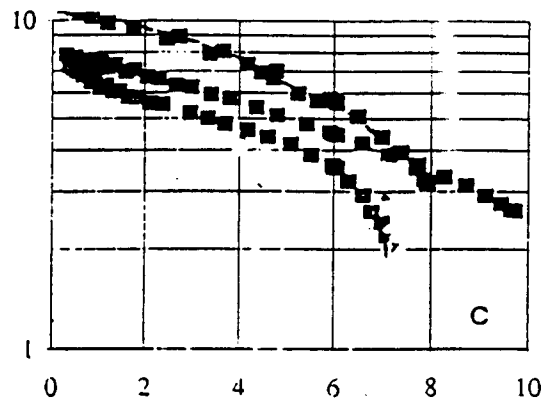

Figure 4 Typical Q (10^9) vs E_{acc} (MV/m) of accepted Nb/Cu cavities for LEP, as measured in vertical test cryostat (from ref. 28).

CERN has developed with success the technique of Nb thin film deposition on copper for the LEP200 cavities [28,29]. The transfer of this new technology to industry has met some difficulties. The chemical treatment of the copper substrate turned out to be a most crucial point, determining the adherence of the Nb film. Local lacks of adherence resulted in "blisters", causing abrupt degradations of the cavity Q value. An appropriate chemical treatment, combined with a dust-free handling of

the Cu substrate brought this problem under control. All three companies involved in the LEP cavity fabrication now deliver cavities with Q values and gradients above the specifications (E_{acc} =6 MV/m, Q_0= 4 10^9 at 4.5 K). These Nb/Cu cavities behave as well, if not better, than massive niobium ones of the same design. Full scale production of the cavities has now started, and the first assembled cryomodules arrive for qualification at CERN.

Thin film samples of the intermetallic compounds NbN, NbTiN and Nb_3Sn are being elaborated in a few laboratories, e.g CERN, Wuppertal or Saclay [30]. Unfortunately, the residual surface resistance of these films is rather high (a few hundreds of $n\Omega$ at GHz frequencies), and increases with increasing RF field. Moreover, the gradients obtained (of the order of 35 mT) are still too low for most applications. The present limitations of performance are probably curable. They are thought to be due to imperfections in the thin film morphology, causing granular superconductivity [31].

Overall, thin films other than Nb/Cu have promising results on samples, but no convincing high-performance cavity has been fabricated yet using these films. The preferred applications of thin film cavities will be focussed on accelerators requiring large duty cycle and small RF dissipation, for which the criterion of high gradient is not a very high priority. Here, thin films open perspectives of simplified cryogenics, since operation of the cavity at high temperatures will be allowed by the very small BCS contribution to the surface resistance.

5. PERSPECTIVES FOR SUPERCONDUCTING C VITIES

SC avity technology is now applied to a wide variety of accelerators, taking advantage of the low RF losses in the cavities. This feature can be exploited in different ways, depending on the particular application under consideration (Table 1). We shall only deal here with the most recent trends and results.

Until recently, the only "low beta" application of RF superconductivity has been for heavy ion linacs. The increasing number of such accelerators indicates that this will continue to be a dominant application. The development of new resonator shapes like superconducting radiofrequency quadrupoles and spoke resonators might open the field: new applications such as high intensity CW ion beams or high duty cycle proton beams for neutron spallation sources are forthcoming.

The advantages of superconducting cavities for accelerators of high luminosity are well known and well documented [1–5]. β = 1 superconducting cavities have been successful in storage rings, and in large duty cycle electron linacs. With the years, these applications are spreading, and becoming more and more convincing. The good news from these last two years is the superb behaviour of the CEBAF cavities. Nearly all cavities tested so far exceed by large amounts the design value (fig. 1).

Accelerator type	Required cavity characteristics
Heavy-ion linacs	Mechanical stability, high gradients
e-linacs with large duty cycle: - for Nucl. Phys. (CEBAF, Darmstadt, ELFE) - for free electron lasers (LISA, HEPL, JAERI...)	Low RF dissipation
High energy hadron rings (LHC, SSC, RHIC)	
High intensity accelerators: - Storage rings (KEK, HERA, LEP200) - Hadron linacs (ESS, AWT...)	Large diameter iris; Couplers with large power handling capabilities
e+ e- linear collider (TESLA)	High accelerating gradient

Table 1 Main applications of SC accelerating cavities

Now, other domains of application are opening, exploiting the advantages of RF superconductivity in other ways:

The idea that RF superconductivity could also be applied to accelerators at the high energy frontier is not new [32], but is gaining strength. The future high energy e+ e- collider might use superconducting cavities. The TESLA collaboration [33], which promotes this idea, has grown considerably during the last two years. Here, the reduced RF dissipation of superconductors is still exploited, but the large diameter beam holes permitted by SC cavities (and the machine parameters which derive from this feature) is probably the most convincing argument in favor of the TESLA project. Altogether, TESLA has already emerged as a credible option for an e+ e- collider in the TeV range. The main challenge of the TESLA cavities will be to reach accelerating gradient of the order of 25 MV/m in 9 cell, 1.3 GHz cavities. The gradients obtained recently in Cornell, Saclay, Wuppertal, CEBAF or KEK suggest that this goal can be reached, but an important amount of R&D will certainly be required to obtain it in a reproducible manner and at low cost.

There is also a new and powerful interest in high intensity hadron linacs, eg for spallation sources. The idea that these accelerators could use superconducting cavities [34] is new and exciting. Here again, the large diameter irises of superconducting cavities are exploited, but this time, the main interest seems to be the reduced activation by the beam halo. These accelerators will necessarily operate at rather low frequency, similar to the

4

LEP frequency (350 MHz). For the same reasons than at LEP, thin film cavities (maybe niobium nitride ?) could be an interesting option for these accelerators.

RF superconductivity is a reliable technology. Some heavy ion linacs or electron rings like Tristan at KEK have already used it for a long time. No long term degradation of the cavity performance have been observed [35]; the essentials of the physical phenomena underlying the behaviour of SC cavities now seem to be understood at the laboratory level. But RF superconductivity is still far from its theoretical limits. The remaining problems are probably of technological order. There is still ample room for improvement, if the present limitations imposed by cleanliness and preservation of the surface quality can be pushed further.

RF superconductivity has reached a stage of validation at the industrial level. One of the main obstacles to the development of this technology is its cost. An important challenge for the future years will be to cut it down.

As far as one can see, the main R&D topics which should be addressed to improve cavities could thus be as follows :

i) field emission, in connection with improved techniques to achieve a good cleanliness of the cavity surface;

ii) thin superconducting films;

iii) improved fabrication techniques, in connection with the metallurgical aspects of Nb elaboration and purification;

6. REFERENCES

1. H. Padamsee, K.W. Shepard and R. Sundelin, Ann. Rev. Nucl. Part. Sci. 43 (1993) 635

2. P. Kneisel, J. Vac. Sci. Technol. A11 (1993) 1575

3. W. Weingarten, Particle World 1 (1990) 93

4. D. Proch, Proc of the 1993 Particle Accelerator Conference, Washington (1993) 758

5. H. F Dylla, L. R. Doolittle and J. F. Benesch, Proc of the 1993 Particle Accelerator Conference, Washington (1993) 748

6. C. Z. Antoine et al. Proc. V[th] Workshop on RF Superconductivity, D. Proch, ed., Hamburg (1991) 456

7. J. Kirchgessner et al., Proc of the 1989 Particle Accelerator Conference, Chicago (1989) 482

8. J. Graber, PhD Thesis, Cornell University, Ithaca (1993)

9. H. Padamsee et al., Proc. V[th] Workshop on RF Superconductivity, D. Proch, ed., Hamburg (1991) 37

10. M. Hörmann, J. Less Common Metals 139 (1988) 1

11. Q. S. Shu et al., NIM A 278 (1989) 329

12. P. Kneisel, J. Less Comm. Metals 139 (1988) 173

13. D. Moffat et al. Cornell report CLNS 89934, Cornell University, Ithaca, NY (1989)

14. J. Delayen and K.W. Shepard, Appl. Phys. Lett. 57 (1990) 514

15. C. Reece et al. Proc of the 1993 Particle Accelerator Conference, Washington (1993) 1016

16. P. Niedermann, "Experiments on enhanced Field Emission", PhD dissertation, Université de Genève (1986)

17. M. Jimenez et al., J. Phys. D: Appl. Phys. 26 (1993) 1503

18. P. Bernard, D. Bloess et al., Proc. of the IIIrd European Particle Accelerator Conference, Berlin (1992) 1269

19. B. Rusnak et al. Proc. of the 1992 Lin. Acc. Conf., Ottawa, C. R. Hoffmann, ed. (1992) 728

20. I. Campisi, IEEE Trans. Mag. 21 (1985) 134

21. A. V. Eliutin et al., Proc. V[th] Workshop on RF Superconductivity, D. Proch, ed., Hamburg (1991) 426

22. B. Bonin and R. Röth, Part. Accelerators, 50 (1992) 59

23. D. Reschke, private communication

24. J. M. Pierce et al. Proc. IXth Int. Conf. Low Temp. Phys. (Plenum press, NY (1965) 396

25. J. Kirchgessner, Proc of the IIIrd Workshop on RF superconductivity (Argonne Ntl Lab. 1988) Report ANL. Phys. 88–1 (1988) p 533

26. V. Palmieri et al., contribution to this conference, and article to be published in NIM (1994)

27. C. Hauviller, private communication.

28. G. Cavallari et al., Proc of the 1993 Particle Accelerator Conference, Washington (1993) 806 and refs. therein.

29. C. Benvenuti et al. XX Int. Conf. on Low Temp. Phys., Eugene, Oregon, USA (1993)

30. P. Bosland et al., Proc. of the Third European Particle Accelerator Conference, Berlin (1992) 1316

31. B. Bonin, H. Safa, Supercond. Sci. Technol. 4 (1991) 257

32. M. Tigner, Nuovo Cimento 37 (1965) 1228

33. H. Padamsee, editor. Proc. of the 1st TESLA Workshop, CLNS report 90–1029 (1990)

34. H. Lengeler, VIth Workshop on RF Superconductivity, ed . R. Sundelin, CEBAF (1993)

35. K. Kubo et al. Proc. XVth Int. Conf. on High Energy Accelerators HEACC 92, ed. J. Rossbach, Hamburg (1992) 691

CEA/DAPNIA/SEA 94 19   07/1994

RF PROCESSING OF FIELD EMITTING PARTICLES

J. Tan, H. Safa, B. Bonin, J. Jodet

RF processing of field emitting particles

J. Tan[a)], H. Safa[b)], B. Bonin[b)], J. Jodet[c)]

a) Thomson Tubes Electroniques, 78141 Vélizy Cedex, FRANCE
b) DAPNIA / SEA, & c) INSTN / SEPEM— Centre d'Etudes de Saclay, 91191 Gif sur Yvette Cedex, FRANCE

Abstract

In this paper, we describe the results obtained from RF field emission experiments on niobium samples polluted with metallic particles. In particular, the influence of the electromagnetic field, the RF pulse length as well as the total number of pulses applied is shown. The peculiar cumulative effect found could bring some new light on the so called high peak power (HPP) processing of cavities.

1. INTRODUCTION

It is now well established that field emission (FE) on broad area electrodes or in radiofrequency (RF) cavities is generally associated with local surface defects such as scratches or contamination particles [1], [2], [3]. Many theoretical models have been developed [4], [5] in order to explain the electron tunneling through the potential barrier at the metal–vacuum interface, for field range two orders of magnitude lower than the theoretical one predicted by Fowler and Nordheim [6]. Lately, FE studies at Saclay [3] showed that the local enhancement of the field can be explained by a modified "projection model"[4] at least for two categories of emitter sites : "intrinsic" sites (i.e. whose composition contains nothing but the substrate's element, e.g. scratches), and "extrinsic" sites (meaning dust particles composed with other foreign species) [2].

Actually a great research effort among the particle accelerators community is undergone to repel FE threshold field. Dealing with scratches, those can be easily removed by means of a "heavy" chemical etching, and one may assume a surface state free of such defects after this treatment.

It had been clearly shown [7], [8] that more cleanliness during the cavity mounting steps led to significant gain for accelerating field. However, the presence of dust particles either in chemical baths or even in cleanroom atmosphere make it more difficult to avoid them on the cavity walls. One proceeds finally to surface treatments *in situ* i.e. with closed cavities.

It is generally believed that RF processing reduces FE by inactivation of emitting sites via a mechanism of thermal instability followed by a microdischarge destroying the site. This mechanism is certainly at work to reduce FE, but we would like to show that HPP processing [9] is also effective to remove mechanically dust particles from the surface, thereby reducing the total FE from the surface.

In a previous paper [10], first experimental results with dust particles obtained with the reentrant 1.5 GHz cavity were reported. Nb samples were intentionally contaminated with iron particles (20–50 μm size) and submitted to an intense pulsed field : 45 MV/m peak with repetition rate $\simeq$ 1 Hz.

We noticed incidentally at that time that the number of remaining particles on the surface after applying the RF power was related to the pulse length. Long pulses led to important thermal effects i.e. melting and welding of the particles on the substrate. After treatment, the proportion of particles remaining on the surface was as follows : 75% for long pulses (τ =10 ms) as compared to 30% for short pulses (τ =100 μs). Thus one might deduce that short pulses were more likely to remove dust particles and then "clean" the surfaces. These observations were consistent with Cornell's group who showed the efficiency of HPP processing for reducing FE in accelerating cavities [9].

Following these observations, we wished to undertake a more systematic study in order to lighten the basic mechanism of "cleaning" dust particles by RF pulses. Three parameters appear to be of major importance :

1. the maximum field level on the surface E_{max},
2. the RF pulse length τ,
3. the total number of RF pulses N.

2. EXPERIMENTAL SET UP

The core of the experimental set up is a re-entrant 1.5 GHz copper cavity working at room temperature. A 5 kW klystron permits application of 50 MV/m peak field on the 10 mm^2 hemispherical top of removable niobium samples. As the cavity is not cooled, the maximum allowed RF power duty cycle is 1 %. Electrons emitted hit a current probe placed 12 mm afar from the sample collecting an *integrated intensity*. Working pressure is better than 10^{-7}mb. The full description of the apparatus, cleaning and operating procedures has been detailed in a previous paper [11].

The purpose of this work is to study the mechanism of particle removal . Thus niobium samples chemically etched are sprinkled with hundreds of iron particles (20–50 μm size) and examined using a scanning electron microscope (SEM) before mounting in the cavity.

RF duty cycle is always kept equal to 1 %. The reference number of particles is arbitrarily taken to be 100 % after an initial low RF field test ($E_{max} \leq$ 5 MV/m) — so as to get rid of uncertainties due to poorly adhering particles that can get lost during transportation between the SEM and the RF cavity. After each RF test, the sample is dismounted from the cavity and observed with the SEM where the number of remaining particles on the surface is counted.

3. EFFECT OF FIELD LEVEL

It has been shown that with a pulse length τ =10 ms and at a field level of 45 MV/m, particles can melt and weld to the sample surface [10]. Therefore, the study of the behavior of

particles as a function of field level should give informations about the optimum field to apply answering the following questions : i/ what is the minimum field required to remove a given particle ? ii/ what is the minimum field to cause an irreversible damage (either by welding the particles or by leaving craters on the surface)?

3.1. Experimental procedure

Four Nb samples were prepared following the procedure described in section 2.2, with different τ values for each, namely 10 ms, 1 ms, 100 μs and 10 μs.

All samples were RF processed at a low field level for 30 mn then removed for SEM observations before applying the higher RF field. Thus all samples experience *successively* 14 MV/m, 30 MV/m and 45 MV/m for 30 mn each time.

3.2. Experimental results

The results are summarized in figure 1. As one could expect, the stronger the field, the lower the number of remaining particles and consequently the more efficient is the "cleaning". More interesting is the fact that at a given field, the shorter the pulse length the better is the cleaning.
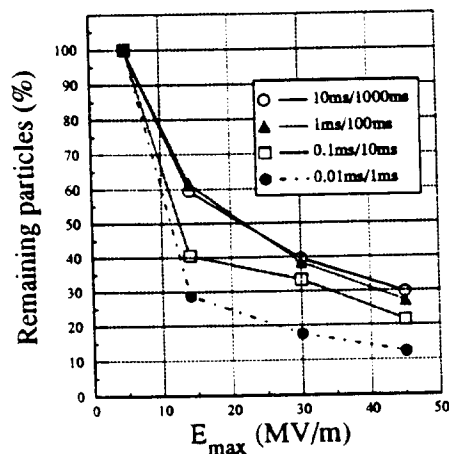
Figure 1. Effect of increasing electric field for different pulse lengths.

3.3. SEM observations

At 5 MV/m, some particles are seen to be lined up along the electric field. Almost all particles seemed in good electrical contact with the substrate as they did not charge under the SEM beam. As the field level was increased, more particles piled up. Below 30 MV/m, no craters were observed on all the samples surfaces with the exception of the sample having the longest pulse length (10 ms) where few craters (about typically 5 μm size) appeared at 30 MV/m. Craters' location was always associated with missing iron particles, and X-ray analysis revealed the presence of Fe element in craters. At 45 MV/m, the number of craters increased with τ.

3.4. FE measurements

Few reliable currents values had been obtained during RF processing. Until 14 MV/m no current signal exceeded the measurement noise (10 pA). For higher field levels, as the working duty cycle chosen was the upper limit for our experiment, microwave heating yielded an important degassing. This led to unstable positive ionization probably near the current probe which altered the current reading. At 30 MV/m the current was generally less than 4 μA whereas it increased to 15 μA at 45 MV/m.

After the last RF tests at 45 MV/m, FE measurements were performed once again at 30 MV/m : significant gain on FE was obtained as the final current did not exceed 1 μA for one sample, and 150 pA for another one.

4. TIME PROCESSING EFFECT

4.1. Experimental procedure

Four other Nb samples were prepared following the procedure described in section 2.2, with different τ values for each (10 ms, 1 ms, 100 μs and 10 μs). After one low field test, all RF tests were done keeping the field constant and equal to 30 MV/m.

We wish to observe whether the total number N of applied RF pulses can modify the number of remaining particles. In other words, is there a cumulative effect of the RF field due to the successively applied pulses and to what extent ? To do so, we apply different time durations t on the same sample, counting after each test, with the help of the SEM, the percentage of the remaining particles. As the effective RF time is $t_{eff} = C \times t$ (C is the duty cycle, here 1 %), the total number of pulses can be evaluated by $N = \frac{t_{eff}}{\tau} = \frac{C \times t}{\tau}$.

4.2. Experimental results

They first confirm the importance of the pulse length that has been already pointed out in the previous section. Short RF pulses are far more efficient than long ones. Moreover, one sees from figure 2 that there is a very strong cumulative effect (at any pulse length) which seems to show no saturation limit : the cleaning of the surface continues as long as the RF power is applied. The longer the time of exposure to RF power, the better will be the processing.
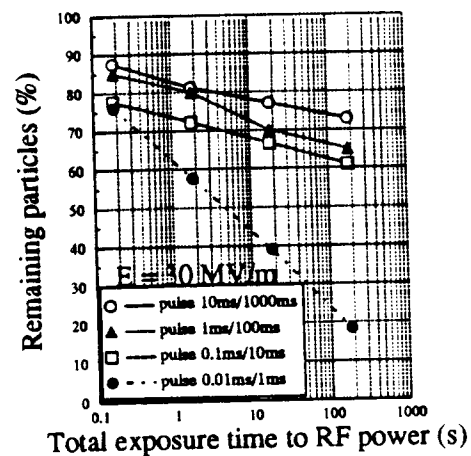

Figure 2. Effect of RF time duration for different pulse lengths.

2

4.3. SEM observations

Figures 3.a and 3.c show the samples before RF tests. In figure 3.b the first sample has undergone 18 s of RF power with a pulse length τ =10 ms, whereas the second sample is shown in figure 3.d after 5 hours of RF power at τ =10 μs. Although the field level was the same for both samples (30 MV/m), one notices that nearly all particles were still lying on the first sample while very few remained on the second one. This clearly proves the efficiency of cleaning with time using very short pulses.

a)   b)

c)   d)
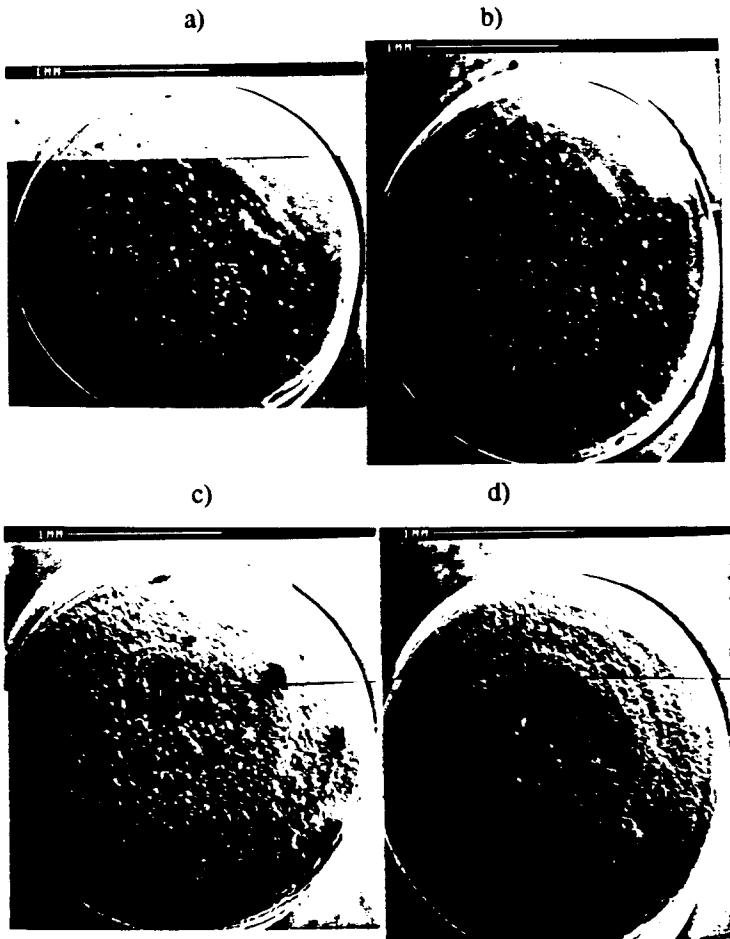
Figure 3. An effective RF processing needs short pulse length and long time : in 3b, the sample shown in 3a before test, has undergone 18s of RF power with τ=10ms. While on another sample (3c before test), 5 hours of processing with 10μs pulses at the same field have nearly clean all particles from its surface (3d after test).

It should also be noted that the surface is much more damaged (craters and molten particles) by long pulses than by short ones, even at the same field and for equal number of RF pulses.

5. DISCUSSION

A first series of experiments confirms the need for high electric field levels to throw away dust particles. Besides, they demonstrate that short RF pulses are also necessary to avoid strong thermal effects that may lead to melting and consequently welding particles onto the surface (generally the contact particle-substrate is very poor). The associated constant time may be easily evaluated and model calculations provides values close to 1 ms [12]. In that view, continuous RF processing for example is expected to be far less effective than pulsed treatments to remove particulate contaminants and to reduce FE.

The second series of experiments suggests that the removal of particulate contaminants by pulsed RF power occurs via a *cumulative mechanism*, and that many pulses of short duration are more effective than a few long ones to clean the surface. In view of this, we predict that medium power pulsed (MPP) processing should be effective to reduce FE, provided the pulse duration and the total processing time are properly chosen.

6. CONCLUSION

This work shows that pulsed RF processing can remove particulate contamination. For that purpose three conditions are required :

— A large number of pulses to obtain cumulative effect,
— Processing with short pulse lengths to avoid welding particles on the surface,
— Applying a high enough peak field to remove particulate.

These new effects contribute to the reduction of FE usually observed after application of "high peak power processing". They should be taken into account in the choice of HPP parameters, favoring (if possible) shorter pulses.

REFERENCES

[1] Niedermann Ph., Ph. D. thesis no 2197, University of Geneva (1986)

[2] Moffat D. et al., Particle Acc., 40, (1992),85–126

[3] Jimenez M. et al., J. Appl. Phys. D, 27, (1994), 1038–1045

[4] Noer R.J., Appl. Phys. A, A28, (1982) 1–24

[5] Latham R.V., IEEE Trans. Elec. Insul., EI23, no 5 (1988), 881–894

[6] Fowler R.H., Nordheim L., Proc. Roy. Soc London. A119,(1928), 173–181

[7] Proceedings of the 2nd Workshop on RF Superconductivity, Geneva, Switzerland (1984)

[8] Proceedings of the 3rd Workshop on RF Superconductivity, New York, USA (1986)

[9] J. Graber, Ph. D. Thesis, Cornell University (1993)

[10] Tan J. et al., Field emission measurements in a radiofrequency field, to be published in J. Phys. D

[11] Tan J. et al., A microwave cavity for field emission studies, to be published in J. Phys. D

[12] Junquera T. et al., Studies on field emission in RF cavities using an optical system, this conference EPAC, London, U.K. (1994)

MAGNETIC SHIELDING OF SUPERCONDUCTING CAVITIES

M. Boloré, B. Bonin, B. Daillant,
O. Delferrieère, J. Faure, S. Jaïdane,
E. Jacques, H. Safa

Magnetic shielding of superconducting cavities

M. Boloré, B. Bonin, B. Daillant, O. Delferrière*,
J. Faure*, S. Jaïdane, E. Jacques, H. Safa

CEA DAPNIA SEA
Saclay F-91191 Gif sur Yvette, France

* CE Saclay Laboratoire National Saturne
91191 Gif sur Yvette Cedex, France

Abstract

In order to reach their nominal performance level, most superconducting cavities must be cooled in a magnetic field smaller than 20–30 mGauss. This corresponds to a field 20 times smaller than the ambient magnetic field in a typical accelerator tunnel. To achieve this shielding level, the use of a mixed scheme, combining a Cryoperm tube around the cavity helium vessel, and a string of Helmholtz coils around the cryomodule vacuum vessel, is recommended.

1. INTRODUCTION

When cooled in an ambient, static magnetic field, superconductors usually trap some flux [1]. In the case of superconducting cavities, this causes undesirable RF dissipation, which must be minimized by a proper magnetic shielding of the cavities. The residual surface resistance caused by flux trapping (for a type II superconductor like Niobium, with a Ginzburg-Landau parameter κ of order unity, and for small trapped flux $B \ll B_{c2}$) is given by:

$$R_s = R_n \frac{B}{B_{c2}}$$

where R_n is the normal-state resistance of the superconductor. In some accelerator applications, like TESLA or ELFE, cavities with low surface resistance are required. The order of magnitude for the tolerable surface resistance due to trapped flux is a few nano Ohms. It is then deduced from the above equation that the level of the residual magnetic field must be brought below 20 mG on the inner cavity surface.

2. PASSIVE MAGNETIC SHIELDINGS

The main contribution to the ambient magnetic field is in general the earth magnetic field, whose magnitude is about 400 mG. The required shielding factor $S = \frac{B_{without}}{B_{with\ shield}}$ must thus lie around 20. A priori, this shielding level may be achievable by means of a simple passive tube of magnetic material around the cavity. For such a tube, analytical formulae exist, giving the shielding factors $S_{\parallel}$ and $S_{\perp}$ for the longitudinal and perpendicular components of the field [2]:

$$S_{\perp} \simeq \frac{\mu.d}{D} + 1$$

$$S_{\parallel} \simeq \frac{4N(S_{\perp} - 1)}{1 + D/2L} \quad \text{closed cylinder}$$

$$S_{\parallel} \simeq 4NS_{\perp} \quad \text{open cylinder}$$

In these equations, μ is the permeability of the tube, D is the tube diameter, diameter, L its length, d the wall thickness and N its demagnetizing coefficient. Application of these equations to the realistic case of a TESLA-type cavity (L=1300 mm, D=250 mm, d=1 mm) show that $S_{\parallel}$=12 and $S_{\perp}$=50 if μ=12000. These values seem to be almost satisfactory. Unfortunately, this too optimistic conclusion must be revised for three reasons:

1) Being close to the superconducting cavity, the magnetic tube will necessarily be cold. Most magnetic materials lose in permeability when their temperature decreases [3]. The only commercially available exception to this trend seems to be Cryoperm. This material, like all other high permeability alloys, is rather delicate to handle. Proper annealings are required to obtain high permeabilities; shocks or strains (either thermal or plastic) can reduce μ drastically.

Altogether, the best choice for a close shielding of superconducting cavities will still be Cryoperm, but measurements made on tube samples show that a realistic value for its permeability at 4 K is only $\mu \simeq 12000$.

2)The above equations neglect end effects. Fringe fields are to be expected at the ends of the tube. Elementary considerations on the conservation of $\int B_{\parallel} dl$ along the cylinder axis indicate that the longitudinal component of the field is depleted in the tube, and is enhanced at the ends of the tube. This enhancement extends over a diameter inside the tube (fig. 1). Calculations with the numerical code BACCHUS [4] indicate that it is possible to reduce the effective diameter of the tube, and thus the range of the fringe fields by adding annular shaped pieces at the end of the tube(s). Unfortunately, this gain in range is more or less compensated by an enhancement of the longitudinal component of the field at the tube ends.

3) In most cases, superconducting cavities are used in closely packed strings. For this reason, a given cavity surrounded by its passive shield cannot be considered as magnetically isolated from its neighbours. The situation of the string is in fact close to the case of a continuous tube of the same total length and diameter. Since the aspect ratio of this "global tube" is very long, the corresponding longitudinal shielding factor will probably be rather poor, necessarily less good than the one evaluated for one single cylinder shielding an isolated cavity.

For these three reasons, it is possible-but rather difficult-to obtain the required level of shielding of the longitudinal component of the field by means of purely passive shields. Calculations made with the finite element code BACCHUS indicate that the gap between tubes is a crucial parameter: if it is too small, the overall shielding factor of the string becomes small because the geometry of the shield becomes close to the shape of a very elongated cylinder with very small demagnetizing coefficient; if the gap is too large, the shielding tubes are not much longer than the cavities, and the fringe fields at the end of the tubes hamper a proper shielding of the cavity end cells.

3. ACTIVE CANCELLATION OF THE FIELD, AND MIXED SCHEMES

In view of these difficulties, it is very tempting to cancel the ambient magnetic field by using active devices, ie coils. The advantages of this option lie in its simplicity and cheapness. Furthermore, the counter-field produced by the coils can be used to degauss any magnetic material in the cavity surrounding, eg the vacuum vessel or any passive shield. Cancellation of the longitudinal component of the field, so difficult with passive shields, can readily be achieved with

a very simple solenoid or string of Helmholtz coils. The perpendicular component of the field are less of a problem, and can be reduced by a purely passive shield.

This "mixed" scheme has been tested in the special case of a TESLA TTF cryomodule, by means of a 1/4 scale model. The vacuum vessel was simulated by a 2 mm thick steel tube. The passive shield was simulated by tubes of Conetic of adequate length and diameter. The permeability of the Conetic was roughly 30000, and the thickness of the tube was d=0.1 mm, chosen so that $(\mu d)_{Model} \simeq scale * (\mu d)_{Tesla}$. The model was oriented North-South, in an ambient magnetic field similar to the one of the TESLA TTF hall. The distribution of the three components of the magnetic field in the model was measured by means of a Förster probe. The field distribution obtained after careful degaussing of the "vacuum vessel" is shown in fig. 1 and Table 1.
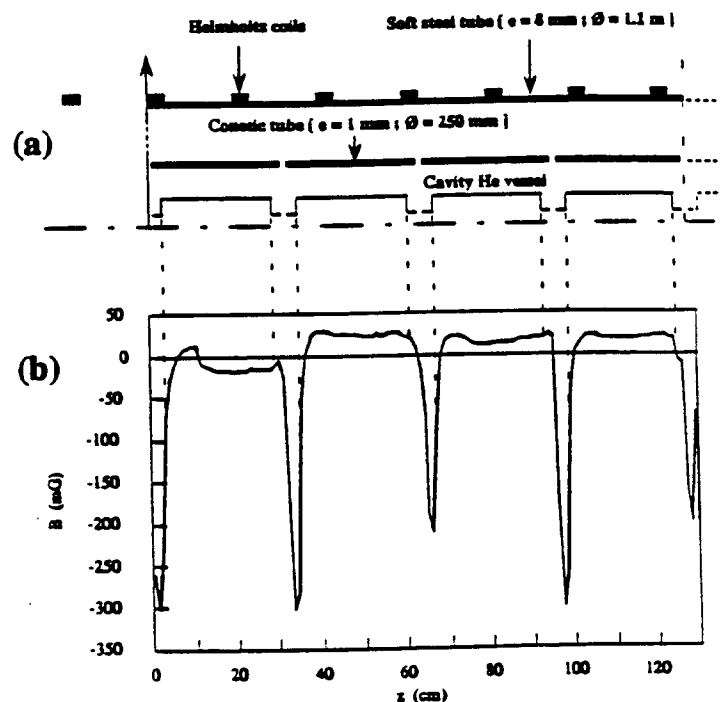

Figure 1. a) A mixed scheme for TESLA TTF cryomodule, b) Field profile measured along the z-axis on a scale 1/4 model

2

	Cavity center	Cavity end cell
$B_\parallel$ (mG)	0±25	0±35
$B_\perp$ (mG)	10±8	15±5

Table 1. Field level measured on the scale 1/4 model of a TESLA TTF cryomodule.

The level of field achieved in the model is quite satisfactory, thus giving much hope that similar results will be obtained with the full scale cryomodule.

4. CONCLUSION

We realized during completion of this work that it is much easier to shield a single cavity than a string of such objects. It is possible that this difficulty had gone unnoticed in the past. We feel, however, that a proper shielding of the superconducting cavities is an indispensable prerequisite to the obtention of high cavity Q-values, and accelerating gradients.

5. REFERENCES

1. C. Vallet et al. EPAC Conference Berlin (1992)

2. A. Mager J. Appl. Phys. 39 (1968) 1914

3. D. L. Martin and R.L. Snowdon Rev. Sci. Inst. 46 (1975) 523

4. The finite element code BACCHUS was developed by CISI engineering for the study of charged particle beams in static electromagnetic fields.

SUPERCONDUCTING, HYDROFORMED, NIOBIUM
SPUTTER COATED COPPER CAVITIES AT 1.5 GHz

D. Bloess, E. Chiaveri, C. Durand,
C. Hauviller, W. Weringarten, P. Bosland,
S. Cantacuzene

Superconducting, hydroformed, niobium sputter coated copper cavities at 1.5 GHz

D. Bloess, E. Chiaveri, C. Durand, C. Hauviller and W. Weingarten
CERN - European Organisation for Nuclear Research
CH–1211 Geneva 23 (Switzerland)

P. Bosland, S. Cantacuzene
CEN Saclay
F-91191 Gif-sur-Yvette Cedex (France)

Abstract

Results from RF tests of five-cell niobium sputter coated cavities are presented. Accelerating gradients of 13 MV/m at low field Q-values of 10^{10} have been obtained. Experimental data on the decrease of the Q-value with accelerating gradient are explained in a model, in which weak superconducting spots are driven normal by the RF field.

1. INTRODUCTION

Superconducting (sc) technology in the 1.3 to 1.5 GHz range may be attractive for future linear colliders in the TeV energy range (TESLA), provided larger accelerating gradients (about 25 MV/m) at high Q-values ($5 \cdot 10^9$) can be obtained at moderate costs. Copper cavities with a thin sc coating of sputtered niobium (NbCu cavities) may offer an alternative to niobium cavities made from sheet, both with respect to costs and to performance. They can be formed in a monolithic piece from a single tube by hydroforming (with intermediate annealing steps), they do not exhibit "quenching" thanks to the high thermal conductivity of copper at low temperature, and the material costs of copper are substantially lower than those of niobium.

However, the RF loss increases more than quadratically with the accelerating gradient (non quadratic loss, NQL), and the copper niobium interface has to be extremely clean to guarantee good adhesion and sufficient cooling of the sputtered film. If not so, minute ($\varnothing \leq 1$ mm) spots of niobium loosely connected to the copper can switch to the normalconducting (nc) state (Q-switch) and even heat up sufficiently that electrons are emitted. This kind of "electron loading" cannot be reduced by "processing".

In what follows we will report on a common effort of CERN and CEN/Saclay to develop 1.5 GHz sc NbCu cavities for large gradients and low RF losses. Previous results have been presented elsewhere [1 - 3].

In particular, two lines of research and development work will be described. Firstly, we will report on results on the feasibility of multi-cell cavities, and secondly on the physics of sputtered layers with the ultimate goal to understand and eliminate NQL.

2. EXPERIMENTAL RESULTS

2.1 Sputtering parameters and reproducibility of results

The sequence of production of the cavity proper, the chemical cleaning and the coating set-up are described elsewhere [3]. Here we will only give information on the sputtering parameters which determine the coating process: anode voltage V, discharge current I, argon gas pressure p, and temperature of the substrate T. All these parameters are intimately connected. Generally speaking, one reduces V to avoid neutral gas resputtering of the film from recoil neutral atoms bouncing off the cathode, which are known to induce constraints in the film. One reduces p to create a dense, non-columnar film. Increasing the power P = IV of the plasma discharge reduces the probability of contamination of the film by gas impurities. It is difficult to take account of all these constraints simultaneously.

Since the new sputtering set-up is available [3], five one-cell cavities and three five-cell cavities have been coated and tested. The coating parameters were not varied significantly, because the reproducibility of the result was to be checked. Prior to coating, the cavities were baked between 100°C and 170°C for 30 minutes. The current I was controlled to about 1.5 A and p between 6 and $7 \cdot 10^{-3}$ mbar. V stabilised around 380 to 410 V and T between 135 and 153°C. Thirty minutes of plasma discharge were needed per cell to produce a layer thickness of 1.6 to 1.8 μm (near the equator and iris of the cavity, respectively), or one hour for twice the thickness.

Four of the one-cell cavities had low field Q-values (at 1.8 K) of $(1.0 \pm 0.2) \cdot 10^{10}$; in three of them the maximum gradient at Q = $1 \cdot 10^9$ exceeded 10 MV/m.

When applying rinsing with ultra pure water at high pressure (high pressure water rinsing HPWR at 90 bar, 12 l/ min mass flow for 75 minutes), some parts of the coating washed off, indicating poor adhesion.

2.2 Feasibility of five-cell NbCu cavities

After hydroforming, the dispersion of the mechanical dimensions was ±0.4‰, and that of the π mode frequencies was ±0.3‰ [3]. The field flatness (defined as the ratio of maximum to minimum field amplitude) was 1.25. After five iterations of inelastic deformations a field flatness of 1.08 could be obtained. Plastic deformation of the cavity was achieved for a longitudinal deformation of individual cells (with the force applied to the irises) corresponding to a change of 500 kHz for the π mode frequency. The measured sensitivity to the helium bath pressure was -40 kHz/mbar.
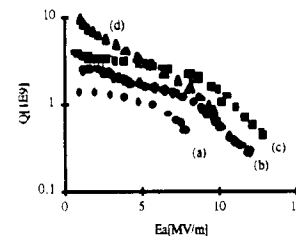

Fig. 1: Q-value vs. accelerating gradient in a five-cell cavity after various treatments: as received after coating (a), after rinsing with ultra pure water at low pressure (b) and high pressure (c, d).

Among the three five-cell cavities, two had poor results: the Q-value decreased steeply with accelerating gradient (due to Q-switches). The thickness of coating was 3.2 to 3.8 μm at the equator and the iris, respectively. The third cavity (thickness 1.6 to 1.8 μm at similar positions) had a Q-value at low field of $4 \cdot 10^9$ and a maximum accelerating gradient of 11 MV/m at Q = $1 \cdot 10^9$ (Fig. 1), the field limitation being electron loading. No attempts have been made so far to decrease the electron activity, no thermal quench was observed. After a second HPWR the low field Q-value increased to more than 10^{10}, but the slope of the Q vs. E_a curve became somewhat steeper. A change of this slope after HPWR has already been observed before [1].

In conclusion, best RF results were similar to those of one-cell cavities, but the success rate (of producing a cavity without major surface flaw as for example a "Q-switch") was 33 %, compared 60 % for one-cell cavities.

2.3 Sample measurements

(a) Critical field B_{c2} and critical temperature T_c:
B_{c2} and T_c are measured inductively with a transformer consisting of two coplanar coils and the sample sheet in between [4]. A DC magnetic field (<3.5 T) parallel to the sample surface is superimposed. When the primary coil is driven AC in the kHz range, a significant voltage is induced in the secondary coil, when the sample is nc. This decreases substantially due to shielding when the sample becomes sc. The secondary voltage is measured vs. the temperature of the sample and vs. the DC magnetic field. A typical result (Fig. 2) shows smeared transitions, both in T_c and in B_{c2}, different from what was observed in bulk niobium. In addition, B_{c2} was significantly larger than for bulk niobium. The RRR of the samples were between 10 to 20.
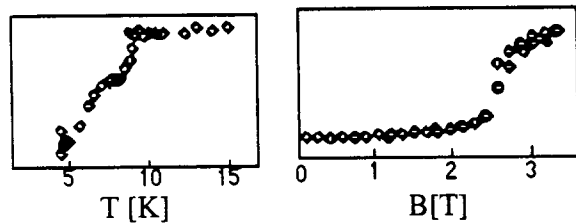

T [K]   B[T]

Fig. 2: Secondary coil voltage (arb. units) for measuring the critical temperature T_c (left) and the upper critical field B_{c2} (right) on a niobium layer sputter coated on a copper substrate. The RRR was 12 for this particular sample, and the temperature during coating was not controlled.

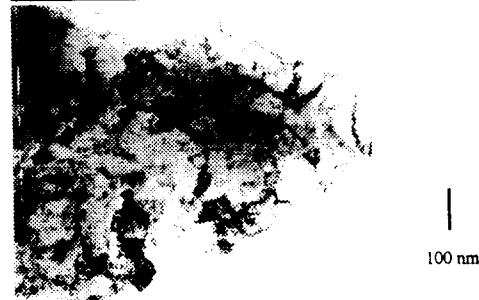(b) Transmission electron microscope (TEM) analysis:

100 nm

Fig. 3: Bright field TEM image of an ion beam thinned niobium sample, which was removed by high pressure water from a sputter coated one-cell cavity.

A sample which was removed from the cavity surface by a blast of HPWR was analysed in a TEM (Fig. 3).

Preliminary results are the following. A large number of grains per unit area are detected, of different size (5 to 200 nm). Within the grains, there are stacking faults and dislocations visible. In an analysis of elemental distribution neither oxygen nor sulphur contamination have been found. If the oxygen had been concentrated near the grain boundaries with a thickness of more than three monolayers, it would have been detected.

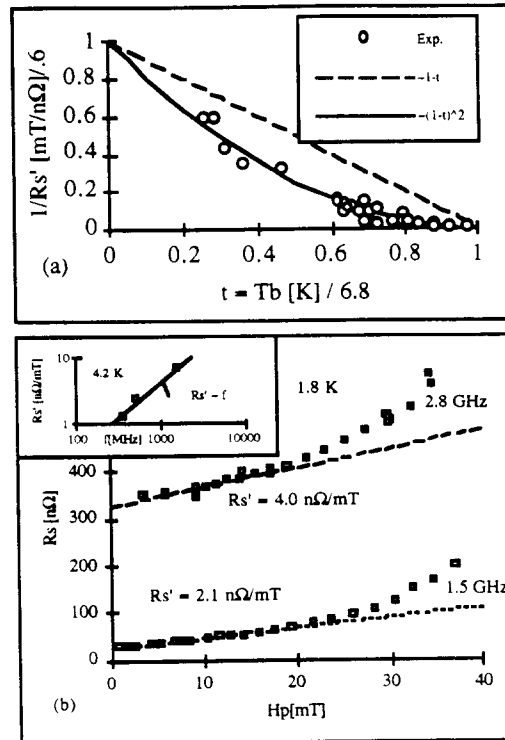### 2.4 Measurements in conjunction with NQL:

Fig. 4: Non quadratic loss (NQL) measured vs. the bath temperature T_b (a) and vs. the RF magnetic peak field amplitude H_p at 1.5 GHz and 2.8 GHz in the same cavity (b).

The losses P generated per m² by a RF magnetic field of amplitude H can be split into magnetic and non-magnetic losses:

$$P = R_s H^2 / 2 + \text{others}, \qquad (1)$$

where R_s is the surface resistance and "others" comprise dielectric loss, electron impact, nc spots, etc.. R_s can be separated into several terms, the BCS and the residual one, which are more or less well known, and another one, named R_s', which takes into account NQL:

$$R_s = R_{BCS} + R_{res} + R_s' \cdot H + \dots \qquad (2)$$

R_s' describes the physical mechanism which create the slope of the Q vs. E_a curve. In order to get more insight into the physics underneath, we have measured the temperature and frequency dependence of R_s' (Fig. 4).

The temperature of the cavity was determined by a calibrated germanium resistor (estimated precision < 0.1 K). The frequency dependence of NQL was measured by exciting not only the

fundamental mode at 1.5 GHz, but also a higher (quadrupole) modes at 2.8 GHz.

The temperature dependence of NQL can be represented by

$$R_s' \propto 1 \Big/ \left(1 - T/T^*\right)^2,$$ (3)

with $T^* = 6.8$ K.

The frequency dependence was linear, contrary to what was indicated in a previous paper [3]. However, evidence now is confirmed by data from NbCu cavities at 4.2 K and 352, 500 and 1500 MHz (inset Fig. 4, b).

3. DISCUSSION

As we have already proposed in a previous papers [5], NQL may be explained by weak sc spots. At that time, we hypothesised oxygen as contaminant, in the form of spots of weak sc phases with depressed T_c. In the TEM analysis we did not find up till now any confirmation for this hypothesis. So we conclude that these weak spots must have a different origin: What we found was a large density of metallurgical defects within grains and a large scatter in grain size. These features are characteristic of granular superconductors, which are composed of (nearly perfect) grains and weak links in between [6].

For those granular superconductors, when lowering the temperature, the grains become sc at the transition temperature of the bulk material. The sample nevertheless is not yet in a phase coherent sc state. This will only happen when the temperature is still lowered and the Josephson "phase locking" temperature T_{cJ} is passed. Then the coupling energy between the grains becomes of the order of the thermal energy kT, such that energy fluctuations can no longer destroy the phase coherence over the whole sample. T_{cJ} can be substantially lower than T_c. It is also known, that the critical field B_{c2} increases with decreasing grain size [7]. These ideas would naturally explain the B_{c2} and T_c measurements on samples at DC.

As to the RF measurements, we define f as that fraction of the surface which the RF magnetic field H has driven nc. We define f_0 that fraction of the surface composed of weak links if $H = 0$. We assume the weak links being nc contribute to the RF loss, and do not contribute at all being sc. By increasing H by a differential amount dH, f will increase by a differential amount df, which in first approximation for small H is proportional to f_0. Hence the relation:

$$df/f_0 = dH/H_c(T),$$ (4)

where the critical magnetic field H_c (T) was introduced for normalisation reasons (f (H_c) = f_0). The surface resistance being proportional to the nc fraction f of weak links, $\alpha \cdot f$ (proportionality factor α), we obtain

$$dR_s/dH = R_s' = \alpha f_0/H_c(T).$$ (5)

H_c (T) corresponds to the critical current j_c (T), by which the weak links are driven nc. Depending on their nature, $j_c(T) \sim T - T_c$ for weak links coupled by an insulator and $j_c(T) \sim (T-T_c)^2$ for weak links coupled by a metal [8]. The former temperature dependence was found elsewhere [3], the latter is found now (eq. 3). Hence we conclude,

$$R_s' = \alpha f_0 \Big/ \left[H_{c0} \left(1 - T/T^*\right)^2 \right].$$ (6)

It comes out naturally that T^* is identical with T_{cJ}.

As to the frequency dependence of R_s it was suggested flux penetrates the intergranular medium in nanoseconds [9]. The energy needed to break the Cooper pairs is delivered by the electromagnetic field. This same energy can probably not coherently be delivered back to the electromagnetic field, when the nc electrons condense again into Cooper pairs. The RF loss is therefore proportional to the number of cycles per second, hence the RF frequency.

4. CONCLUSION

We have shown that maximum gradients of 13 MV/m and low field Q values of $Q > 10^{10}$ can be obtained in five-cell cavities. Thermal quenching was not observed, the limitation of the gradient was electron loading. These results are not significantly different from what has been obtained in one-cell cavities, despite the fact that in five-cell cavities the probability of having defects of poor adhesion is larger.

In the second part of the paper we have given an analysis of the decrease of the Q-value with the accelerating gradient in terms of weak links switching into the nc state by the action of the RF field.

REFERENCES

[1] Ph. Bernard et al., Proc. 5th Workshop RF Superconductivity, 19-23 August 1991, DESY, Hamburg (Germany), ed. D. Proch, 487.

[2] Ph. Bernard et al., Proc. 3rd European Part. Acc. Conf., Berlin (Germany), 24-28 March 1992, eds. H. Henke, H. Homeyer, Ch. Petit-Jean-Genaz, 1269.

[3] Ph. Bernard et al., Proc. 6th Workshop RF Superconductivity, 4-8 October 1993, CEBAF, Newport News VA (USA), ed. R. Sundelin, in press.

[4] W. Weingarten et al., CERN/EF/RF 87-2.

[5] G. Arnolds-Mayer and W. Weingarten, IEEE Trans. Magn. MAG-23 (1987)1620.

[6] J. Clem, Physica C 153 - 155 (1988) 50.

[7] M. Tinkham and C. J. Lobb, Solid State Physics 42 (1989) 91.

[8] P. G. de Gennes, Superconductivity of Metals and Alloys, New York 1966, 238.

[9] A. M. Portis, Proc. Earlier and Recent Aspects of Superconductivity, Erice (Sicily), Italy, 4-16 July 1989, ed. J. G. Bednorz and K. A. Müller.

ELABORATION AND CHARACTERIZATION OF Nb AND
 NbTiN SUPERCONDUCTING THIN FILMS FOR *RF*
APPLICATIONS

S. Cantacuzene, P. Bosland, J. Gobin,
       M. Juillard, J. Martignac

Elaboration and characterization of Nb and NbTiN superconducting thin films for RF applications.

S. Cantacuzène, P. Bosland, J. Gobin, M. Juillard, J. Martignac
CEA, Direction des Sciences de la Matière, DAPNIA/SEA
CE Saclay, F-91191 Gif sur Yvette Cedex, France

Abstract

This paper presents the last results obtained at Saclay on Nb and NbTiN coatings prepared by magnetron sputtering for making 1.5 Ghz accelerating cavities. The optimisation of the sputtering parameters was made on small samples, and the surface resistance of the films deposited on Φ 12 cm copper disks was measured using a TE011 cavity. The results obtained (R_{res}=40 nΩ at T=1.4 K and F= 4 Ghz for the best NbTiN coating) encouraged us to deposit such films in 1.5 GHz copper cavities. One Nb/Cu and four NbTiN/Cu cavities have been prepared, the copper cavities being electrochemically polished before sputtering. The Nb/Cu cavity reached 12.5 MV/m with Q_0=10^{10} at low field. The NbTiN cavities could not be tested because of the blistering of the coatings.

1. INTRODUCTION

For the future accelerators, the technology of the sputter coated cavities appears as an interesting alternative to the bulk Nb superconducting cavities. Nevertheless , even if Nb sputtered cavities are already used for the 350 MHz cavities of the LEP project, important progress is still needed for the 1.5 GHz Nb and NbTiN sputtered cavities so as to become really competitive. That is why an intensive study started in 1986 at the C.E.Saclay was meant to develop and to optimize the technological process for making 1.5 GHz sputter coated copper cavities.

A magnetron sputtering setup, designed to prevent dust contamination of the cavity before sputtering was realized. In the mean time a new magnetron cathode designed so as to allow the variation of the atomic Nb/Ti ratio was also developed. Details on the setup and the cathode were previously reported elsewere [1],[2]. Several Nb sputtered monocells and pentacells cavities were prepared using this setup, and were tested at CERN. The good results obtained during this collaboration with CERN showed that the sputtering setup worked satisfactorily [2]. The selected material for the study was the NbTiN which, due to its higher critical temperature (between 16 K and 17 K), presents a lower BCS surface resistance at 4.2K than Nb [3],[4].

In this comunication we present the major results on NbTiN samples that helped to define the process parameters, the RF behavior of the NbTiN film measured using the TE011 cavity and some preliminary results on 1.5 GHz Nb/Cu and NbTiN/Cu cavities.

2. NbTiN SAMPLE RESULTS

NbTiN films deposited on polished SiO_2 substrates were used to measure the film critical temperature and its room temperature resistivity using a 4 points probe method. The film thickness was measured using a Taly-step

device.The thickness of the sputtered NbTiN films was between 0.7 and 4 μm.

Chemical analysis were made for very thin films (<5000 Å deposited on polished graphit samples) using RBS and NRS technics [5], and for thicker films (1 μm to 15 μm deposited on copper samples) using GDS (Glow Discharge Spectroscopy).

All the NbTiN films have been prepared on the new sputtering setup (mentioned in the introduction) which had only been used for Nb coatings before. An exhaustive study of the sputtering parameters was thus necessary (as we did with our first setup in ref [1],[4]).

The curves on figure 1 show that there is an optimum value of the nitrogen flow for which the film has the highest critical temperature and the lowest resistivity at room temperature. Nevertheless this optimum value changes if we modify the parameters of the glow discharge.
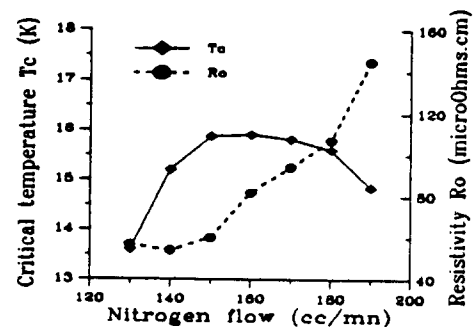

Figure 1: *typical variation of the film's critical temperature and resistivity at room temperature versus the nitrogen flow. For this example the argon flow was 250 cc/min (partial pressure of 7*10^-3 mbar), the glow discharge power was P=600W, the film thickness was 1.7μm and the atomic Nb/Ti ratio was 0.52/0.48. The deposition speed is constant with the nitrogen flow (420±20 Å/min).*

We observed, like other authors [6], that the optimum value of the nitrogen flow is proportional to the power applied to the magnetron cathode. In addition we observed that the deposition speed (and thus, the metal atoms flow at the substrat's surface) is proportional to the magnetron power (figure 2). This confirms a result which is commonly observed in magnetron sputtering.

It is then clear that these two parameters, magnetron power and nitrogen flow (or nitrogen partial pressure), are the two main parameters controlling the reaction between the Nb or Ti atoms and the nitrogen ones. To obtain the good stoechiometric composition of the film (one nitrogen atom for one metal atom) the flows of metal and nitrogen atoms impinging the substrat's surface must be carefully adjusted.

Argon partial pressure, substrate temperature, magnetron cathode temperature, cathode-substrate distance

and pumping speed are also important, especially to minimize the film internal stress. The high rate of internal stress may cause the coating's blistering, when the adhesion with the substrat is poor (this will later be detailed for the NbTiN films sputtered inside some copper cavities). Therefore , all parameters have to be choosen carefully and their large number makes this optimization step quite complex.

One of the basic questions in reactive sputtering is to know whether the reaction takes place on the substrate surface, on the magnetron cathode surface, or during the transport of the metallic vapor between the two surfaces. The results described hereafter seem to show that the reaction might take place on the cathode surface.

\ Three samples have been deposited at the same time at different distances from the magnetron cathode: d=7, 8 and 12.5 cm. The range of the deposition speed of these films (and thus the sputtered metal atoms flow on the substrate surface) varies by a factor of 3.18 following a low in $1/d^2$, whereas the nitrogen flow depends only of the nitrogen partial pressure and is therefore the same for the three samples. The critical temperatures of these films are respectively 16.15, 16.04, and 15.95 K, whereas for films deposited with the same deposition speed a 20 % variation of the nitrogen flow leads to a drastic decrease of the Tc values (shown on figure 1).
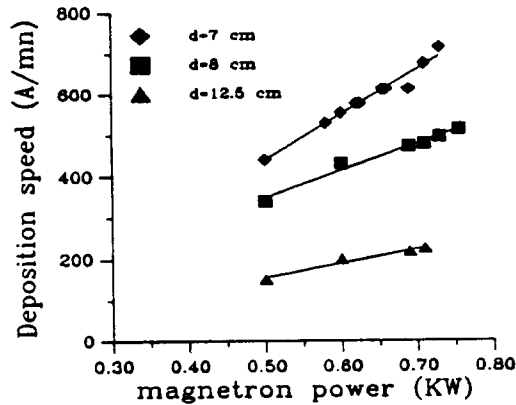

Figure 2: *the deposition speed versus the power of the glow discharge for three cathode-substrate distances (d). Argon and nitrogen partial pressures were kept constant ($p_{Ar}=7*10^{-3}mbar$ and $p_{N2}=2.5*10^{-3}mbar$). A correction based on the cosine low was used each time a substrate was sputtered under an angle.*

We observed that for constant nitrogen flow, discharge power and substrate temperature, the film's critical temperature and resistivity were fairly constant regardless of the film's thickness (over 1μm).

The NbTiN films thinner than 1μm presented a lower critical temperature and a higher resistivity. This might be due to the fact that the samples reach a thermal equilibrium only after ~30min of deposition. An other possible explanation is the fact that at the begining of the sputter process the film is sligtly contaminated (O,H,C) by the adsorbed gases on the samples' surface and by the residual pressure of H_2O and CO_2. After the first micron is sputtered, the film plays a gettering role and the next microns of the layer contain less impurities.

3. RF CHARACTERIZATION USING THE TE011 CAVITY

In the next paragraphs we present the follow up of the RF characterizations made with the TE011 cavity developed at Saclay. This cavity and the method applied for the RF tests had already been described in detail previously [1]. In our last communication [1] we presented two main results:

- the first was the low residual surface resistance obtained (figure 3: $R_{res}=40$ nΩ for F= 4 Ghz and T=1.6 K) at low field level and the maximum RF field level $B_{max}=34$ mT.

- the second was the large spread of the R_{res} values measured on different NbTiN coatings: from 40 nΩ to 2000 nΩ at low field level.

We observed after the RF tests that the copper substrates had been deformed during mounting on the TE011 cavity. We increased the copper disk's thickness from 2 mm to 3 mm to diminish the deformations, and the spread of the RF results obtained on the next NbTiN coatings was considerably lowered as shown on figure 3.
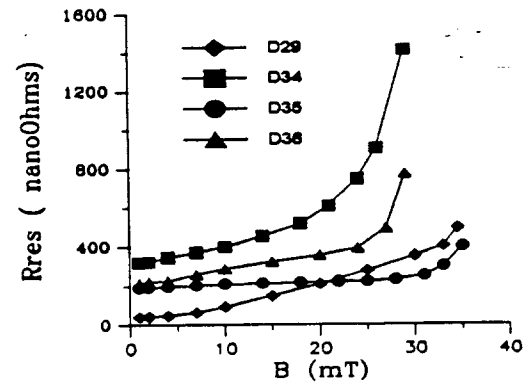

Figure 3: *Residual surface resistance of the last three NbTiN films deposited on 3 mm thick copper substrats compared to our best result previously obtained (D29)*

One hypothesis to explain the mechanical deformations' influence over the surface resistance could be the creation of micro-cracks on the NbTiN films surface. It is well known that the magnetron sputtered nitrides are brittle and cracks may appear under small deformations of the substrate. A great number of such micro-cracks could be the cause of RF dissipations. The confirmation of this hypothesis is of prime importance. It can be made by the analysis of the toughness of the films which we haven't done yet [7].

4. RESULTS ON 1.5 GHZ COPPER CAVITIES

Single cell copper cavities have been hydroformed at CERN [2]. Before sputtering, the copper cavities have been mechanically and then electrochemically polished. In figure 4 we describe the main elements of the electropolishing setup. The cavity is horizontaly placed (like on the KEK system for Nb polishing [8]), half filled with H_3PO_4 acid mixed with water and revolves around its axis at a speed of 3-5 turns per minute. The cathode, reproducing the cavity's shape, is fixed at a distance of 2-3

cm from the cavity's inner surface. A membrane, fixed all around the cathode, guides the H_2 bubbles to the upper half of the cavity. The current density is 5 A/dm^2. After the electrochemical treatment, the cavity is rinsed in ultra pure water, chemically treated with sulfamic acid and then rinsed again with utra pure water and dried in a class 100 clean air room. The film is afterwards prepared following the process described in ref [2].
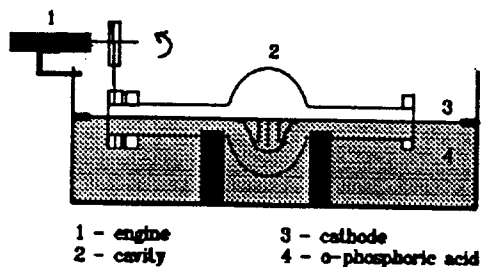

1 - engine   3 - cathode
2 - cavity   4 - o-phosphoric acid

<u>Figure 4</u>: *electropolishing system*

4-1. Results on 1.5 GHz Nb/Cu cavities

Before sputtering any NbTiN coatings, we decided to prepare a Nb coated cavity so as to test the copper electrochemical treatment. After sputtering, the Nb coating was rinsed with ultra pure water and dried in a class 100 clean air room. The RF measurements are presented on figure 5. At T=1.6 K, $Q_0=10^{10}$ at low field level and decreases with the RF field down to $6.5 \ 10^8$ at $E_{acc}=12.5$ MV/m, limited by the amplifier. The cavity was not limited by Q-switches or by electrons. We will not discuss here the slope of the curve on figure 5, which is generaly observed with sputter coated cavities [9],[10] and interpreted in terms of granular superconductivity. This good result encouraged us to prepare NbTiN/Cu cavities using the copper's electrochemical polishing treatment.

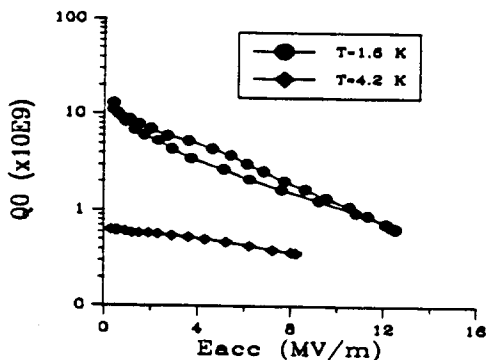*4-2. Results on 1.5 GHz NbTiN/Cu cavities.*

<u>Figure.5</u>: *RF measurements of S1-03 Nb/Cu cavity.*

Four NbTiN/Cu cavities were sputtered but unfortunately none could be tested. Indeed, the film's internal stress and probably the local poor adhesion caused the coating's blistering for all the cavities.

The process parameters were modified between the first and the last of the four cavities. External copper temperature was kept under 70°C during the process and argon partial pressure was incresed up to 10^{-2} mbars, which diminished the film's stress.

The sulfamic acid treatment was supressed and this seemed to somehow ameliorate adhesion.

Progress between the first and the last of the sputtered cavities is obvious but effort is still needed for process improvements.

5. CONCLUSION

Several sample studies have stressed the potential of NbTiN for RF applications. Process parameters were analysed and optimised working points were defined. Reproductibility of the RF surface resistance was studied on a TE011 cavity. The different sequences of the elaboration of 1.5 GHz sputter coated cavities (electrochemical polishing, rinsing, sputtering and final rinsing) were tested and work in a satisfactory manner.

We have obtained for the first Nb/Cu cavity a quality factor of $Q_0=10^{10}$ at low field level, and a maximum field of $E_{acc}=12.5$ MV/m without Q-switches or electron loading. The first series of NbTiN/Cu sputtered cavities could not be tested as the layer had several square milimeters blistering. Nevertheless, important progress is actualy being made.

6. REFERENCES

[1] - P.Bosland et al , Proc. 6th Workshop on RF Supercond. 1993, CEBAF , Newport News V.A. (USA),ed. Sundelin.

[2] - Ph. Bernard et al , Proc. 6th Workshop on RF Supercond. 1993, CEBAF , Newport News V.A. (USA),ed. Sundelin.

[3] - R. Di Leo et al , J.Low Temp. Physics , vol 78 , n°1/2 , pp 41-50 ,1990.

[4] - F.Guemas , thesis , 1992 Paris XI - Orsay, (France)

[5] - B. Roux et al. Nucl.Instr.and Meth. in Ph. Reserch B64 pp184-188, 1992, (North-Holland)

[6] - J.Danroc et al , Int.Symp. on Trend. and new app. and Thin Films , Strasbourg , pp 16-20 , 1987

[7] - J.H. Selverian and al., Thin Solid Films vol 235 pp 120-128, 1993

[8] - K. Saito et al , Proc. 4th Workshop on RF Supercond., vol.2, 1989, KEK, Tsukuba (Japan)

[9] - B.Bonin et al. , Supercond. Science Technol. vol 4, pp 257-261, 1991

[10] - D.Bloess and al., this workshop.